Department of Biomedical Sciences

University of Veterinary Medicine Vienna

Institute of Medical Chemistry

(Head: Univ.-Prof. Dr.rer.nat. Florian Grebien)

Effects of Δ^9-tetrahydrocannabinol on the modulation of mitochondrial activity in neuroblastoma cells

BACHELOR THESIS

For obtaining the degree

Bachelor of Science (BSc.)

Of the University of Veterinary Medicine Vienna

Submitted by

Lea Charlotte Klein

Vienna, June 2022

Supervisor: Dipl.-Biol. Dr.rer.nat. Rudolf Moldzio

Reviewer: Ao.Univ.-Prof. Dr.rer.nat. Lars Gille

Declaration

I declare that the work for this Bachelor thesis was only carried out by myself, apart from the determination of effective concentrations of modulators, which I did in collaboration with Ms. Nadine Stranzl, another bachelor's applicant. The information I derived from the literature is acknowledged in the text, and a list of references is provided. No other literature has been used. I declare that I have written this thesis independently, and it was not submitted or published elsewhere.

Vienna, July 04, 2022

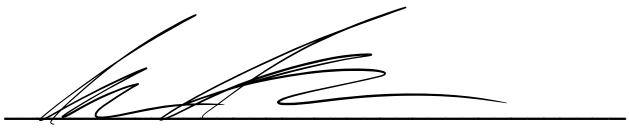

Lea Charlotte Klein

Summary

Cannabis sativa has been used for medical applications for over 5.000 years. Over the last decades, many studies have reported neuroprotective properties of Δ^9-tetrahydrocannabinol (THC), though the mechanisms leading to those effects are not fully understood. What is widely accepted is that some of those properties emerge from the ability of THC to bind to cannabinoid receptor 1, which is also present in mitochondria.

THC has also been shown to protect mitochondria against inhibitors of the complex I of the electron transport chain. Subsequently, THC-based medicine has been discussed for clinical neurological use for diseases in which mitochondrial impairment occurs, e.g., Parkinson's disease or Alzheimer's disease. Since mitochondria have their own cannabinoid receptors 1, it is hypothesized that THC could also directly impact mitochondrial functions.

This study aims to reveal if and where neuroprotective properties of THC occur within the electron transport chain. For this purpose, the oxygen consumption of THC-treated murine neuroblastoma cells was measured using a sensor-based OxoPlate®, and the mitochondrial membrane potential was observed through the fluorescent dye JC-1. In this cell culture system, effective concentrations of the complex I inhibitor rotenone and the uncoupler carbonyl cyanide m-chlorophenylhydrazone (CCCP) could be determined, while unexpectedly, administration of the ATP synthase inhibitor oligomycin did not have a significant effect on the cells.

THC only had minimal effects on the cells and on their reaction following inhibitor-induced toxicity. CCCP treatment did lead to a significant increase in the oxygen consumption. This effect was observed from the beginning in THC-treated cells, too, but was only significant in control cells after 15 minutes. Although the present data does not explain the neuroprotective properties of THC against mitochondrial impairment, the results of CCCP-treated cells support the hypothesis that there is a direct impact of THC on mitochondrial functions.

Zusammenfassung

Cannabis sativa wird seit über 5000 Jahren medizinisch verwendet. In den letzten Jahrzehnten haben viele Studien neuroprotektive Eigenschaften von Δ^9-tetrahydrocannabinol (THC) vermeldet. Die Mechanismen, die zu diesen Effekten führen sind jedoch weitgehend unverstanden. Bestätigt ist, dass THC einen Teil seiner Wirkung über die Bindung an den Cannabinodrezeptor 1 vermittelt, der auch auf Mitochondrien zu finden ist.

Vorausgehende Studien haben gezeigt, dass THC Mitochondrien vor Komplex I Inhibitoren der Elektronentransportkette schützt. Seither steht THC-haltige Medizin in der Diskussion gegen neurodegenerative Krankheiten, wie Morbus Parkinson oder Morbus Alzheimer, eingesetzt zu werden. THC verlangsamt die Entwicklung dieser Krankheiten; daher wird vermutet, dass THC die Zellen in eine Art Ruhezustand versetzt. Da Mitochondrien auch Cannabinodrezeptoren 1 besitzen, wird vermutet, dass THC eine direkte Wirkung auf sie zeigt.

Diese Studie möchte zeigen, ob und falls ja, wo die neuroprotektiven Eigenschaften an der Elektronentransportkette auftreten. Dafür wurde der Sauerstoffverbrauch von mit THC behandelten, murinen Neuroblastomzellen mittels einer Sensor-basierten OxoPlate® gemessen und das mitochondriale Membranpotential wurde durch den Fluoreszenz-Farbstoff JC-1 überwacht. In diesem Zellkultur-System konnten effektive Konzentrationen des Komplex I Inhibitor Rotenon und des Uncouplers Carbonylcyanide-m-chlorophenylhydrazone (CCCP) gefunden werden. Unerwarteter Weise führte eine Behandlung mit dem ATP-Synthase Inhibitor Oligomycin zu keinem erkennbaren Effekt.

THC hatte nur geringe Effekte auf die mit Inhibitoren behandelten Zellen. Die Behandlung der Zellen mit CCCP führte zu einem signifikanten Anstieg in ihrem Sauerstoffverbrauch. Dieser Effekt war bei mit THC behandelten Zellen von Anfang an signifikant, während unbehandelte Zellen erst nach 15 Minuten mehr Sauerstoff verbrauchten. Obwohl die heutige Datenlage die neuroprotektiven Eigenschaften von THC gegen mitochondriale Schädigung nicht erklärt, unterstützen die Ergebnisse der CCCP-Behandlung die Hypothese, dass THC einen direkten Einfluss auf Mitochondrien hat.

Abbreviations

ATP	adenosine triphosphate
mtDNA	mitochondrial DNA
ROS	reactive oxygen species
IMS	intermembrane space
Acetyl CoA	acetyl coenzyme A
ETC	electron transport chain
MMP	mitochondrial membrane potential
PD	Parkinson's disease
CCCP	carbonyl cyanide m-chlorophenylhydrazone
ECS	endocannabinoid system
CBD, CBDA	cannabidiol. cannabidiolic acid
THC, THCA	Δ^9-tetrahydrocannabinol, Δ^9-tetrahydrocannabinolic acid
CB_1R	cannabinoid receptor 1
CB_2R	cannabinoid receptor 2
GPCR	G-protein-coupled receptors
TRPV1	cation channel subfamily V member 1
PPARS, PPARγ, PPARα	peroxisome proliferator-activated receptors/ -γ/-α
GDP	guanosine diphosphate
GTP	guanosine triphosphate
AEA	anandamide
2-AG	2-aranachidonoyl-glycerol
PKA	protein kinase A
AMPK	AMP-activated protein kinase
CBMPs	cannabis-based medicine products
DMEM	Dulbecco's Modified Eagle's medium
FBS	fetal calf serum
DMSO	dimethyl sulfoxide
PBS	phosphate buffered saline
PDL	poly-D-lysin hydrobromide
BSA	bovine serum albumin
JC-1	5,5′,6,6′-Tetrachloro-1,1′,3,3′-Tetraethyl-imidazolocarbocyanine Iodide

Table of Contents

1 Introduction

1.1 Mitochondria

Mitochondria are organelles that enable eukaryotic cells to perform adenosine triphosphate (ATP) synthesis on a greater scale than through glycolysis alone. Mitochondria originated from symbiotic bacteria, at some point taken up by a eukaryotic progenitor (Nunnari & Suomalainen, 2012). Like their bacterial ancestors, they possess a circular genome. However, most of their genes are now encoded by the nucleus after their approximately two billion years-long courses of their co-evolution (Wallace, 2012). Of the over 1,500 proteins thought to be associated with mitochondria and their functions, only 13 are encoded by mitochondrial DNA (mtDNA), while the rest of the genes reside within the nucleus. Mitochondria are involved in and influenced by many cellular processes and operate closely with the rest of the cell (Nunnari & Suomalainen, 2012).

Besides the production of energy in the form of ATP, they modulate the oxidation-reduction potential, control Ca^{2+} levels in the cytosol and participate in the biosynthesis of membrane components (such as cardiolipin) and other cellular substrates (Alberts et al., 2015; Wallace, 2012). They are involved with programmed cell death and innate immune responses. Reactive oxygen species (ROS), derivates of molecular oxygen, are produced by mitochondria and play an essential role in cell signaling at physiological levels (Sies & Jones, 2020). Impairment of mitochondrial functions can have significant consequences. High concentrations of ROS can lead to oxidative stress and DNA damage, inducing cancer development. Other diseases associated with mitochondria can be attributed to dysfunctional signaling pathways, including neurological disorders, cardiovascular disease, and diabetes (Kirtonia et al., 2020). The close relationship between mitochondria and their bacterial ancestors makes them prone to antimicrobial drugs. For example, targeting bacterial ribosomes through antibiotics lead to a stop of the translation of mtDNA, and antiviral nucleoside analogs interfere with mtDNA replication. This suggests that antimicrobial therapies can be genetic risk factors for mitochondrial diseases (Nunnari & Suomalainen, 2012).

The essential function of mitochondria is the production of energy by oxidative phosphorylation, which is crucial for eukaryotic life. Mitochondria have two membranes, lipid bilayers with

distinct lipid and protein compositions. They separate reaction compartments which enable the mitochondrial energy production using an electrochemical gradient. The outer mitochondrial membrane is not curved to a great extent and contains many porin molecules that create pores large enough to let ions and small molecules up to 5000 Dalton pass. The inner membrane, on the contrary, is impermeable to ions and small molecules and is heavily folded, forming so-called cristae. The inner mitochondrial membrane contains the mitochondrial matrix. The space between the membranes (the intermembrane space, IMS) and the matrix create the primary reaction site (Alberts et al., 2015).

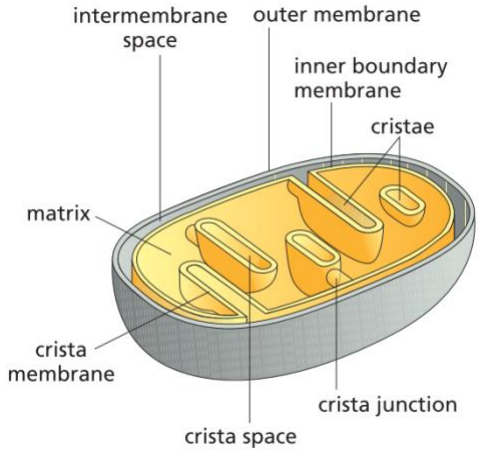

Figure 1: Mitochondria
Schematic illustration of a mitochondrion. The crista membrane is also known as the inner mitochondrial membrane
(Alberts et al., 2015)

Pyruvate (from glycolysis), fatty acids and amino acids are imported from the cytosol and transported across the inner mitochondrial membrane by specific transporters, such as the mitochondrial pyruvate carrier (Bender & Martinou, 2016; Wallace, 2012). Enzymes in the mitochondrial matrix can then use those molecules as substrates to produce acetyl coenzyme A (acetyl CoA). Acetyl CoA enters the citric acid cycle in the matrix and is ultimately oxidized to produce CO_2 and electron carriers, such as NADH and $FADH_2$. Those carriers function as substrates in the electron transport chain (ETC) (Wallace, 2012).

1.1.1 The Respiratory Chain

The ETC, also called the respiratory chain, comprises four protein complexes situated in the cristae. Together with the ATP synthase, they produce energy by oxidative phosphorylation. The individual complexes, including the ATP synthase, will be described in more detail below.

Complex I, or the NADH-ubiquinone oxidoreductase, is the largest protein complex in the ETC. The central function of the complex is the transfer of electrons from NADH to ubiquinone and the subsequent reduction of ubiquinone to ubiquinol using two protons. This leads to a conformational change and the pumping of four protons into the IMS. The complex is L-shaped

and resorts from two multiprotein domains: a membrane arm and a matrix arm. While the membrane arm is situated inside the inner membrane, the matrix arm reaches out into the cytoplasm. The matrix arm contains seven subunits, a flavin mononucleotide located at the cytosolic end of the protruding arm, and several iron-sulfur clusters (Zhao et al., 2019). The membrane arm comprises multiple subunits, of which three (ND2, ND4, ND5) resemble antiporters. The central axis of this domain contains a wire of water molecules (Kampjut & Sazanov, 2020). Only recently, it was understood how the conformational change of the complex, after ubiquinone binding, can move four protons across the inner mitochondrial membrane. NADH from the citric acid cycle binds at the flavin mononucleotide and donates two electrons. This pair of electrons is then passed along the chain of iron-sulfur complexes to subunit N2 and subsequently to ubiquinone, which binds in a cavity, a substructure of the membrane arm close to the joint of the matrix arm. Protons only cross the membrane in the subunit farthest away from the ubiquinone binding cavity. In contrast, the other two antiporter-like subunits facilitate a linkage between ubiquinone and the subunit involved in moving the protons across the inner mitochondrial membrane (Kampjut & Sazanov, 2020). While the ubiquinone cavity is unbound, a helix blocks the water wire in the inner membrane domain. The conformational changes that occur through the binding of ubiquinone lead to a rotation of the helix, the water wire can form, and a connection between the subunits is obtained. Two protons reduce ubiquinone to ubiquinol, creating a charge at the antiporter nearest to the cavity. This charge moves along the subunits in an electrostatic wave, facilitated by the water wire, leading to the translocation of the protons (Kampjut & Sazanov, 2020).

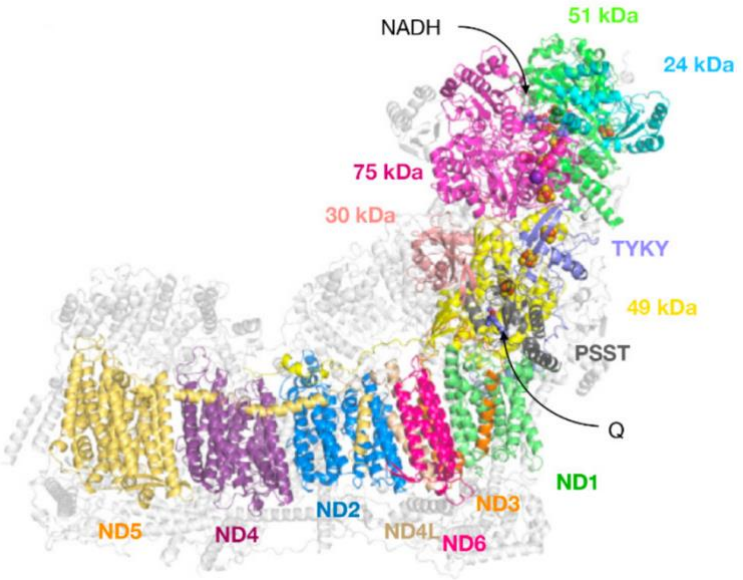

Figure 2: Complex I
Core subunits of the complex are displayed in color. Binding sites of NADH and ubiquinone (Q) are indicated by the black arrows (Kampjut & Sazanov, 2020)

Complex II, also called the succinate dehydrogenase, is not only part of the ETC but also partakes in the citric acid cycle, where it oxidizes succinate to fumarate. Succinate donates two electrons to FAD, leading to its reduction to $FADH_2$ (Sousa et al., 2018). Similar to complex I, complex II, consisting of four subunits, can accept electrons from $FADH_2$ and move them between iron-sulfur clusters before donating them to ubiquinone. Ubiquinone is reduced to ubiquinol, but no protons are pumped into the IMS at complex II (Zhao et al., 2019).

Complex III or the ubiquinone-cytochrome *c* reductase is involved in transferring electrons from ubiquinol to cytochrome *c*. It is a dimer, with each monomer composed of 11 subunits with cytochrome *b* (two b-type hemes: b_L and b_H), cytochrome c_1 and an iron-sulfur cluster being the catalytic active ones. The first electron transferred from ubiquinol, provided by complex I and II, is accepted by the Rieske iron-sulfur protein. It gives the electron to cytochrome c_1, a protein that transfers the electron to cytochrome *c*, a carrier (Sousa et al., 2018). The electron donation from ubiquinol results in the formation of unstable radical ubisemiquinone. Ubisemiquinone can produce superoxide by transferring its remaining electron to oxygen, though most of the time, it is accepted by the heme groups (b_L and b_H) of cytochrome *b*. Ubisemiquinone gives its electron to heme b_L, subsequently giving it to heme b_H. Heme b_H then reduces ubiquinone to ubisemiquinone on the matrix side. Another ubiquinol molecule enters the cycle from the IMS, gets diminished in the same manner, and donates its final electron to ubisemiquinone to form ubiquinol on the matrix side (Chandel, 2010). This leads to the pumping of two protons into the IMS for every oxidized ubiquinol molecule (Nolfi-Donegan et al., 2020).

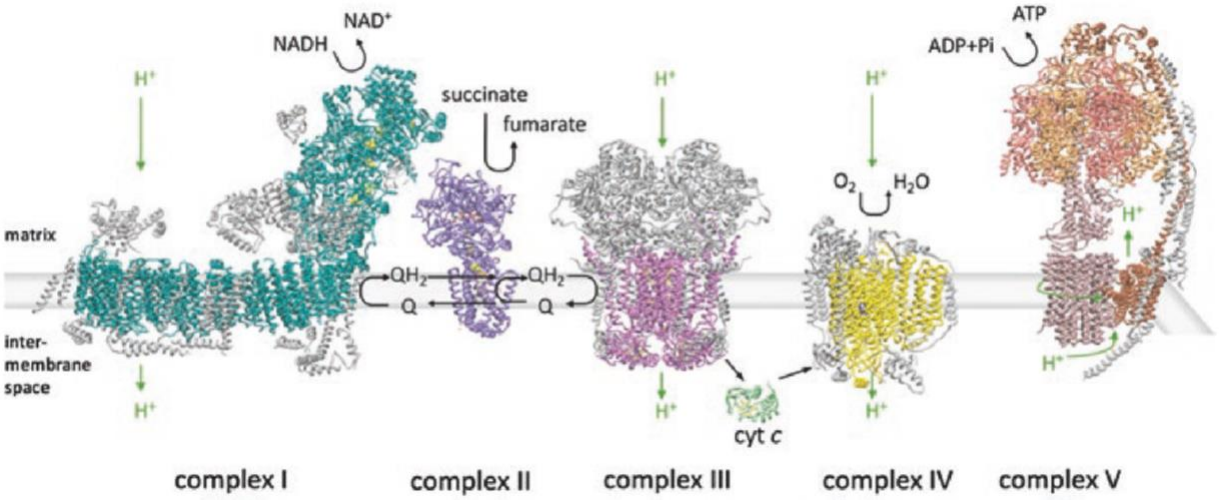

Figure 3: The complexes of the electron transport chain
Core subunits of the complexes are displayed in color. Green arrows indicate H^+ pumping. Black arrows indicate substrate conversion. Ubiquinon (Q), Ubiquinol (QH_2), cytochrome c (cyt c) conversion can be seen (Sousa et al., 2018)

Complex IV also named the cytochrome *c* oxidase, is the last proton pumping complex. It is composed of 14 different subunits and possesses four catalytic sites. Three of those cofactors are located in subunit I: heme *a*, heme a_3 and Cu_B. Subunit II contains the final catalytic site Cu_A. Heme a_3 and Cu_B together form the binuclear center, which can take up two electrons when complex IV is in its reduced state (Sousa et al., 2018). The reactions of complex IV can be divided into two phases, a reductive phase, and an oxidative phase. The reductive phase starts with an oxidized complex IV that accepts two electrons from two cytochrome *c* molecules, leading to a reduced state of the complex. The following oxidative reaction leads to the formation of H_2O from O_2. O_2 first binds onto the complex, reacting with the binuclear site. Two other cytochrome *c* molecules donate another electron to the complex, respectively (Sousa et al., 2018). Altogether, eight protons are taken from the matrix side. Four protons and four electrons are ultimately transferred to O_2, leading to the formation of H_2O and an oxidized complex. The other four protons are transferred to the IMS (Zhao et al., 2019).

The ATP synthase, also called complex V, utilizes the proton gradient, also called mitochondrial membrane potential (MMP), produced by the previous complexes. This enzyme possesses two major protein domains, F_0 and F_1, resembling rotors (Sousa et al., 2018). The segments are held in the same orientation through a peripheral stalk, comprised of multiple subunits of both F_0 and F_1. The F_0 segment is inserted in the inner membrane and comprises various subunits, including subunit *a* and the c-ring (Guo & Rubinstein, 2022). The F_1 segment protrudes into the matrix. F_1 consists of three α, three β and, respectively, one γ, δ, and ϵ subunit (Zhao et al., 2019). The γ subunit is partly embedded into the F_0 segment and an active part of a rotor, leading to the translocation of the complex following the rotation of the γ subunit. Three nucleotide-binding pockets can be found on the β subunits. Two of those pockets are bound most of the time, usually by ADP or AMP-PNP, a non-hydrolysable AMP analog, or two of those molecules, respectively. The third site is very different from the others and rarely bound (Sousa et al., 2018). The F_0 segment obtains its energy from the translocation of protons from the IMS and the F_1 segment utilizes ATP hydrolysis as an energy source. Protons in the IMS pass through the F_0 segment, and the energy stored by the proton gradient is transferred by subunit *a* and the *c*-ring to F1. Protons from the IMS utilize proton channels in these subunits to pass to the matrix side. This ionic current causes the rotation of the γ subunit, leading to a conformational change in other subunits of F_1 (Guo & Rubinstein, 2022). ATP is produced from ADP and inorganic phosphate in the binding pockets through oxidative phosphorylation (Zhao et al., 2019).

1.1.2 Model Compounds for Investigating Mitochondrial Function

The role of mitochondria in the cell makes the understanding of their functions necessary to accurately predict their role in disease. Inhibitors of mitochondrial function can give insight into their operation. Modulation of their operation can help in finding therapeutic targets. Additionally, mitochondria have become a cancer therapy target in recent years (Cui et al., 2017). Several model compounds have been found, of which three are described below.

1.1.2.1 Rotenone

Rotenone is a potent complex I inhibitor of the ETC. It was previously used in pesticides and naturally occurs in roots and stems of the *Derris* and *Lonchocarpus* species (Heinz et al., 2017). It is highly toxic to fish and insects because of the direct uptake of the toxin from the environment of the respiratory system. The toxicity in mammals is not as high since uptake mainly occurs through the digestive tract, where rotenone is broken down into less toxic metabolites (Mpumi et al., 2016). Rotenone binds at three sites of complex one, the ubiquinone binding cavity, a quinone binding site associated with the uptake of quinone, or the ejection of quinol, and the antiporter subunit ND4 (Kampjut & Sazanov, 2020). This leads to impaired oxidative phosphorylation and ATP production. Additionally, rotenone can lead to the production of ROS and further damage to the mitochondria and cells. As a complex I inhibitor, rotenone became widely used in Parkinson's disease (PD) research (Heinz et al., 2017; Radad et al., 2019).

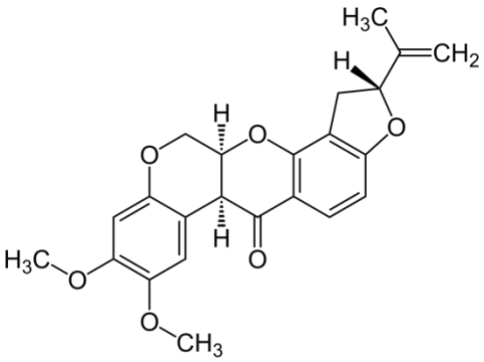

Figure 4: Chemical structure of rotenone (https://commons.wikimedia.org/wiki/File:Rotenone_Structural_Formula_V.1.svg#/media/File:Rotenone_Structural_Formula_V.1.svg)

1.1.2.2 CCCP

Carbonyl cyanide m-chlorophenylhydrazone (CCCP) is an uncoupling agent that increases the inner mitochondrial membrane permeability (Kane et al., 2018). The uncoupler leads to a depolarization of the MMP by facilitating the free reflux of protons through the inner mitochondrial membrane, resulting in mitochondrial dysfunction (Kwon et al., 2011). Studies showed that CCCP gets distributed according to its transmembrane concentration gradient. In the matrix, CCCP dissociates into $CCCP^-$ and H^+. $CCCP^-$ then passes across the inner mitochondrial membrane back into the IMS, again following its concentration gradient. $CCCP^-$ binds to H^+ in the IMS and CCCP diffuses back into the matrix (Plášek et al., 2017). It has also been reported that oxygen consumption increased following CCCP treatment (Mills et al., 2016). Additionally, treatment with CCCP can induce mitophagy and autophagy and increase AMP kinase activity, resulting in cell death (Koncha et al., 2021).

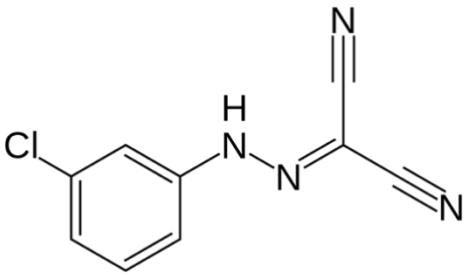

Figure 5: Chemical structure of CCCP (https://commons.wikimedia.org/wiki/File:Carbonyl_cyanide_m-chlorophenyl_hydrazone.svg#/media/File:Carbonyl_cyanide_m-

1.1.2.3 Oligomycin

Oligomycin is an antibiotic that impairs cellular respiration by inhibiting the ATP synthase. It disables the ATP synthase by inhibiting the proper coupling of the oligomycin-sensitivity conferring protein. This protein sits at the top of the F_1 domain and connects it with the peripheral stalk and, thereby, F_0 (Antoniel et al., 2014). Oligomycin also binds at subunit 9 of the F_0 segment, preventing protons from passing through it (Artika, 2019). Thus, oligomycin stops both ATP synthesis and the translocation of protons through the ATP

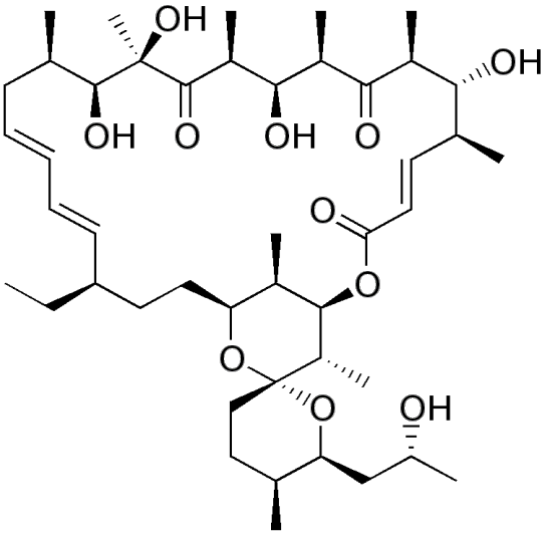

Figure 6: Chemical structure of oligomycin (https://commons.wikimedia.org/wiki/File:Oligomycin_A.png#/media/File:Oligomycin_A.png)

synthase. This leads to a rapid increase in the MMP and a stop of the respiratory chain, stopping O_2 consumption by oxidative phosphorylation (Hearne et al., 2020). The remaining oxygen consumption is associated with the low-level leakage of protons across the inner mitochondrial membrane, the production of reactive oxygen species and other cellular processes (Keuper et al., 2014; Ruas et al., 2016). Recently it has been shown that oligomycin can also lead to an uncoupling of the proton transportation from ATP-synthesis and a return of the oxygen consumption rate to normal levels after some time. Although the mechanisms behind this recovery of the oxygen consumption rate are not fully understood, the authors propose that the effects of oligomycin are more complex than previously assumed (Hearne et al., 2020).

1.2 The Endocannabinoid System and Phytocannabinoids

The endocannabinoid system (ECS) and phytocannabinoids are connected through their discovery. Usage of *Cannabis sativa* plant components, commonly known as marijuana or hemp, has been described over millennia (Zou & Kumar, 2018). The earliest report of medical application dates back to ancient China, approximately 2,600 years BC, where it was known for its benefits in reducing pain (Maroon & Bost, 2018; Zou & Kumar, 2018). The phytocannabinoids, cannabidiol (CBD) and Δ^9-tetrahydrocannabinol (THC) were discovered and identified as the primary metabolites by the 1960s (De Petrocellis & Di Marzo, 2009; Maroon & Bost, 2018). Of the about 120 phytocannabinoids recognized, THC was determined to be the main psychoactive component of *Cannabis sativa* and subsequently more studied (Zou & Kumar, 2018). This led to the discovery of two receptors from the late 1980s to the 1990s, using analogues of Δ^9-tetrahydrocannabinol (THC) as ligands (Cristino et al., 2020; De Petrocellis & Di Marzo, 2009). Given their interaction with THC, the receptors were named cannabinoid receptors. The complex system - comprised of endogenous ligands, enzymes involved in their biosynthesis and degradation, and other receptor – that has been subsequently discovered was titled the ECS (Di Marzo & Piscitelli, 2015; Lowe et al., 2021; Zou & Kumar, 2018). The ECS has become a popular subject of research for pharmacological therapy in the last decades, given its great applicability for many different diseases, including

pain relief, asthma, mood and anxiety disorders, neuropsychological and neurodegenerative diseases such as PD, and cardiovascular diseases (Lowe et al., 2021; Maroon & Bost, 2018).

1.2.1 The Endocannabinoid System

The great efforts put into studying the ECS revealed its complexity. Apart from its receptors, ligands (endocannabinoids) and enzymes involved in the metabolism of endocannabinoids, mediators of the ECS significantly affect other cellular and metabolic pathways. Those cross-reactions lead to the discovery of an even bigger entirety of proteins and pathways affected by the ECS's components: the endocannabinoidome. Those complex interactions have hindered or slowed the identification of therapeutic targets that do not exhibit other unwanted effects upon their activation (Cristino et al., 2020). The most notable characteristics of the ECS are described in more detail below.

1.2.1.1 Cannabinoid Receptors, Endocannabinoids and Metabolizing Enzymes

The ECS possesses two primary receptors called the cannabinoid receptor 1 (CB_1R) and the cannabinoid receptor 2 (CB_2R), although other receptors have been identified that react with cannabinoids. Both CB_1R and CB_2R are G-protein-coupled receptors (GPCR), though other receptors described include ion channels and nuclear receptors, such as the cation channel subfamily V member 1 (TRPV1) and the peroxisome proliferator-activated receptor-γ and -α (PPARγ, PPARα) (Cristino et al., 2020; Zou & Kumar, 2018).

GPCR, and therefore CB_1R and CB_2R, can regulate the activity of different enzymes through their associated G protein, following the binding of their corresponding signal molecule. The G protein consists of three subunits. The α subunit is bound with guanosine diphosphate (GDP) upon activation. When the signal molecule binds the GPCR, GDP is exchanged with guanosine triphosphate (GTP). The G protein subsequently undergoes a conformational change, leading to the split of the βγ subunit from the α subunit. Both parts can act on a diverse quantity of proteins, such as enzymes or proton channels (Alberts et al., 2015).

CB_1R is thought to be the most abundant receptor in mammalian brain tissue (Cristino et al., 2020). Two isoforms of CB_1R exist, resulting from alternative splicing of the corresponding gene (Zou & Kumar, 2018). The concentration of CB_1R is highest in parts of the brain associated with memory, emotion, pain and movement. This is supported by the great density of the receptor in regions of output basal ganglia (including the substantia nigra pars reticulata and segments of the globus pallidus), the dentate gyrus and the cerebellum (Maroon & Bost, 2018). Furthermore, CB_1R is also expressed in skeletal muscle, liver, pancreatic tissue, and central and peripheral nervous systems, especially GABAergic neurons, but the expression in glutaminergic neurons is lower (Lutz, 2020; Maroon & Bost, 2018; Zou & Kumar, 2018). CB_2R is not as commonly distributed as CB_1R but is heavily associated with the immune system (Cristino et al., 2020). Two isoforms have been discovered; one is primarily detected in the testis, the other predominantly in the spleen and peripheral immune cells (Lutz, 2020; Zou & Kumar, 2018). Both isoforms are also found in the brain (Zou & Kumar, 2018). CB_2R is highly expressed in microglia present in diseases such as Alzheimer's disease (Cristino et al., 2020). CB_2R is also found in hippocampal glutamatergic neurons and dopaminergic neurons of the ventral tegmental area (Lutz, 2020).

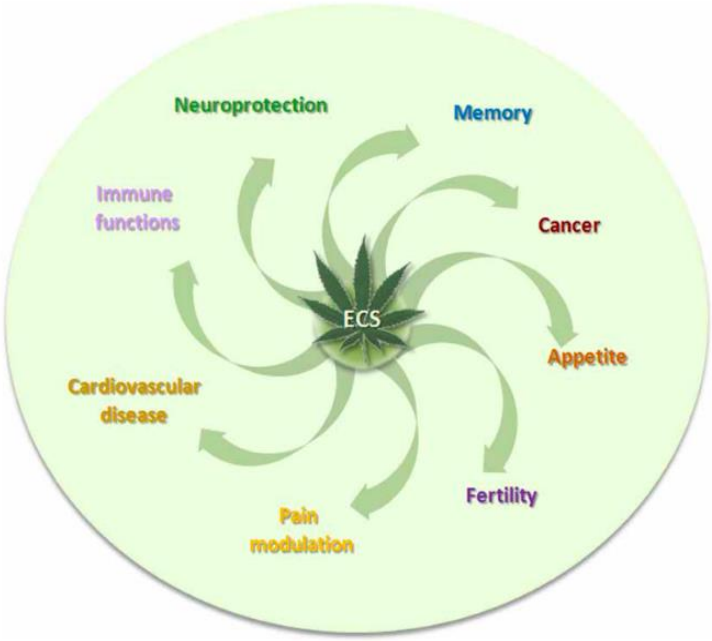

Figure 7: Pathophysiological conditions with involvement of the ECS
(Battista et al., 2012)

Endocannabinoids can also act on other receptors. They can lead to the activation of the TRPV1, PPARγ and the ion channel $GABA_A$ (a diverse class of inotropic receptors with the endogenous ligand γ-aminobutyric acid) (Cristino et al., 2020; Wisden et al., 2019). Additionally, they can inhibit $Ca_{v3.2}$ Ca^{2+} channels and transient receptor potential cation channel subfamily M member 8 channels (TRPM8) (Cristino et al., 2020).

Anandamide (*N*-arachidonoyl-ethanolamine; AEA) and 2-aranachidonoyl-glycerol (2-AG), classified as lipids, are the most well-known endogenous ligands of the cannabinoid receptors (Cristino et al., 2020; Zou & Kumar, 2018). While AEA is an agonist for CB_1R, 2-AG can act on both major receptors and is therefore thought to be the primary ligand. CB_1R-interacting peptides. Other endocannabinoids have been discovered but remain relatively understudied (Zou & Kumar, 2018). AEA has stimulating effects on TRPV1 and PPARγ and hindering effects on $Ca_{v3.2}$ Ca^{2+} channels and TRPM8, while 2-AG can activate TRPV1 and $GABA_A$ (Cristino et al., 2020).

The primary role of endocannabinoids is the suppression of synaptic transmission. AEA and 2-AG are produced after the intracellular calcium concentration is increased. Both neurotransmitters are hydrophobic and uncharged; they cannot diffuse through the postsynaptic membrane; their transport systems are not fully uncovered. After the release into the synapse, 2-AG and AEA bind to CB_1Rs on the presynaptic terminal. The calcium-influx stops and the release of neurotransmitters ceases. However, AEA predominantly binds at intracellular CB_1Rs. The function of CB_2R is not as well understood, but it is believed that the opening of Ca^{2+}-activated chloride channels following the receptor activation leads to reduced neuronal firing (Zou & Kumar, 2018).

1.2.1.2 Cannabinoids and Mitochondria

G protein-coupled CB_1 receptors are also located on mitochondrial membranes, where their function is associated with the regulation of the mitochondrial energy (Joshi & Onaivi, 2019; Lutz, 2020). Mitochondrial CB_1R is not only expressed in neurons but is also found in the mitochondria of spermatozoa and other peripheral tissues. Its exact location within the mitochondrial membranes (outer, inner, or both) is still unknown (Herbert-Chatelain et al., 2017). Endocannabinoids can directly impact mitochondrial energy generation and decrease mitochondrial respiration and thereby ATP production (Herbert-Chatelain et al., 2017). Studies showed that endocannabinoids impaired ATP production through the manipulation of the ATP synthase. Additionally, they decrease the MMP, leading to a lower H^+ gradient across the membranes (Lipina et al., 2014). Although the mechanism through which cannabinoids can impact mitochondria is not fully understood, many different effects of cannabinoids in mitochondria have been observed. Phytocannabinoids are known to induce apoptosis by

processes such as ROS production and receptor modulation (Herbert-Chatelain et al., 2017; Rimmerman et al., 2013). At complex I, cannabinoids can regulate complex activity through the modulation of the mitochondrial protein kinase A (PKA) (Lutz, 2020). It was also hypothesized that endocannabinoids could alter mitochondrial function through intracellular calcium levels. While binding of ligands to CB_1R leads to lower calcium levels, activation of TRPV1 can increase the intracellular calcium concentration, subsequently leading to higher or lower cell metabolism. Furthermore, it was proposed that CB_1R can lead to the activation of the AMP-activated protein kinase (AMPK), which leads to the replacement of damaged mitochondria or apoptosis as a cellular stress response. Endocannabinoids also impact mitogen-activated protein kinase and cAMP pathways, leading to further cooperation of mitochondria and the ECS (Nunn et al., 2012). Degradation of AEA and 2-AG has been observed in mitochondria and high levels of FAAH were detected, suggesting further fundamental connections between the ECS and mitochondria (Herbert-Chatelain et al., 2017).

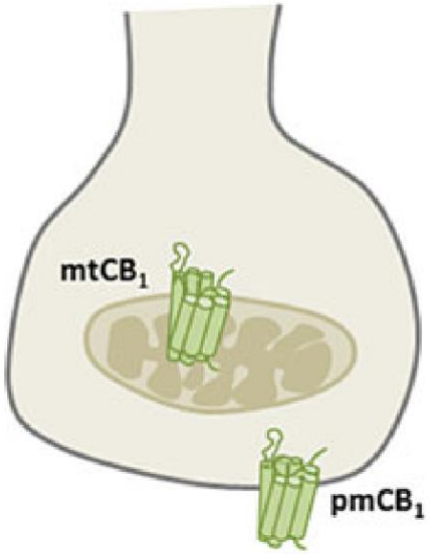

Figure 8: Localization of CB_1R
Mitochondrial CB_1R ($mtCB_1$) and plasma membrane CB_1R ($pmCB_1$) are displayed (Herbert-Chatelain et al., 2017)

1.2.2 Phytocannabinoids

The phytocannabinoid group consists of over 120 different cannabinoids, including their metabolites, primarily found in *Cannabis sativa*. In drug hemp, the most abundant phytocannabinoid is Δ^9-tetrahydrocannabinolic acid (THCA), with cannabidiolic acid (CBDA) prevailing in hemp used for its woody fibers. Phytocannabinoids are mainly found in female flowers, while their concentration depends on the variety and age of the plant and growing and harvesting conditions. Phytocannabinoids emerge from two pathways in the plant that produce acids of the components. Those acids have to be decarboxylated enzymatically or physically (by heat) to develop most of their pharmacological properties, although pharmacological properties of THCA have been reported (Andre et al., 2016; Nadal et al., 2017).

1.2.2.1 Δ^9-Tetrahydrocannabinol

THC binds with a higher affinity at the CB_1R, but it can also act as a agonist at the CB_2R. It is produced by the THCA synthase that produces THCA from cannabigerolic acid (CBGA). CBGA acts as a precursor not only for THCA but also for CBDA and other phytocannabinoids, but the enzymes involved in their generation are different (Andre et al., 2016). In the body, THC is mostly degraded into 11-hydroxy-THC (11-OH-THC) and 11-carboxy-THC (11-COOH-THC) by the hepatic enzyme cytochrome P450 (CYP450) isozymes CYP2C9, CYP2C19 and CYP3A4. 11-OH-THC and 11-COOH-THC are glucuronidated and eliminated through urine and feces. THC has an initial fast half-life (six minutes) with a longer terminal half-life of approximately 22 hours, which is attributed to the tissue distribution (Lucas et al., 2018).

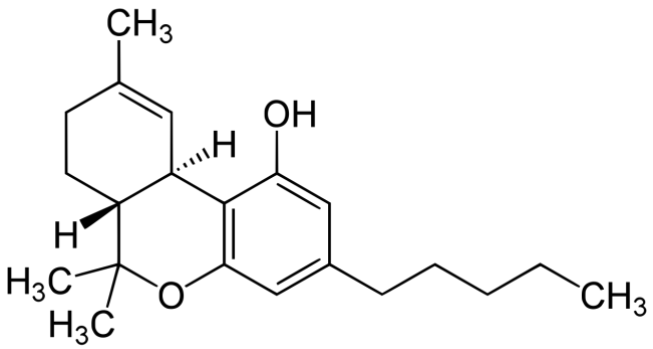

Figure 9: Chemical structure of THC (https://commons.wikimedia.org/wiki/File:Tetrahydrocannabinol.svg#/media/Datei:Tetrahydrocannabinol.svg)

THC has psychoactive effects and can lead to a dose-dependent impairment of cognitive and psychomotor abilities. It can produce psychotic symptoms such as altered perception and increased anxiety levels. Cannabinoid consumption is also linked to tachycardia (Lucas et al., 2018). It is also known for its appetite stimulation and anti-inflammatory and immune-suppressive characteristics. Cytokine and chemokine production is downregulated upon consumption (Lowe et al., 2021). Most of its effects are thought to be directly associated with the interaction of THC with CB_1R and CB_2R. However, given the complexity of the ECS, phytocannabinoids, much as their endogenous analogs, have diverse impacts (Cristino et al., 2020).

Today cannabis-based medicine products (CBMPs) are again in use after they were banned as narcotic drugs for many years in almost the whole world. In most US states and over 20 countries, cannabinoids can be prescribed today (Lucas et al., 2018). CBMPs can range from, most often, purified THC and CBD to mixtures of those cannabinoids and other components of *Cannabis sativa*. Notably, many studies reported better results using a combination of CBD

and THC than using the components independently. Many diseases, which report promising results from the use of CBMPs, are not widely distributed like PD, Tourette's Syndrome, and Dementia. Therefore, data is spare. Other promising applications are involved in treating Substance Use Disorders and anxiety. CBMPs have high strength in their evidence when applicated to treat nausea in cancer patients, stimulate appetite and reduce pain (Schlag et al., 2021). Stimulation of mitochondrial CB1R has been found to convey obesity; blocking of CB1R lead to reduced body weight in mice. Therefore, CB1R is thought to be associated with energy metabolism, and interest in using CBMPs as a treatment for obesity was created (Lipina et al., 2014).

In models of Huntington's disease, neuroprotective properties of THC were observed. It has been proposed that THC can have additional indirect and direct effects on peroxisome proliferator-activated receptors (PPARs). These receptors are involved in numerous processes such as analgesic and neuroprotective effects and neuronal function modulation. Additionally, THC can have antitumor and cardiovascular effects (Maroon & Bost, 2018). In Alzheimer's disease, treatment with THC and a cyclooxygenase 1 inhibitor led to a reduction of β-amyloid plaques and improved neuronal fitness (Maroon & Bost, 2018). Beside other mutations, mitochondrial impairment has been linked to the onset of PD (Nunnari & Suomalainen, 2012). Treatment of both THC and CBD lead to enhanced memory function. In PD, treatment with THC lead to an improvement of symptoms (Cristino et al., 2020). In cell cultures, THC treatment showed apparent neuroprotective properties; in PD models of monkeys, nearly pre-disease levels of locomotor skills (such as walking) were obtained upon treatment (Cooray et al., 2020).

Due to its neuroprotective properties, THC and other phytocannabinoids, such as CBD, are under consideration to become potential drugs used in medical applications (Lowe et al., 2021). Considering that CB_1R is present in mitochondria and the ECS involvement in neurodegenerative diseases that also involve the impairment of mitochondrial functions (such as PD), it has been hypothesized that THC and cannabinoids have a direct impact on mitochondria (Lipina et al., 2014; Nunnari & Suomalainen, 2012).

1.3 Aims

Based on previous findings, THC is hypothesized to modify mitochondrial action. This could be due to a direct interaction with proteins of the mitochondrial respiratory chain or binding to mitochondrial CB_1 receptors ($mtCB_1Rs$). The aim of this study was to shed light on the neuroprotective properties of THC on the ETC in neuroblastoma cells. For this purpose, the three modulators of the ETC rotenone, CCCP and oligomycin were tested.

Mitochondrial activity was assessed through two methods. Staining of cells with JC-1 provided information about the MMP, while OxoPlate® measurements gave insight into the oxygen consumption of cells.

The following questions should be answered:

I. Which concentrations of the modulators are necessary to generate significant differences in the mitochondria and their operation?

II. Does THC treatment change the mitochondrial reaction to those modulators?

III. Does THC exhibit effects against the modulators, which may point to possible sites of action of THC where the modulators interfere with the normal cell functions?

2 Materials and Methods

2.1 Material

2.1.1 Cells

N18TG2 cells, German Collection of Microorganisms and Cell Cultures, Germany

2.1.2 Equipment

Magnetic stirrer, big squid [white], Ika, Germany

Incubator, NAPCO Model 5410, Germany

Incubator, Cell Xpert, Eppendorf, Germany

Microscope, Nikon Diaphot 300, Japan

Vortex 1, IKA, Germany

Counting chamber Neubauer improved, Bartelt, Austria

Lamin Air Holten, Bartelt, Austria

Laminar Flow HERAsafe®, Kendro Laboratory Products, Germany

Centrifuge, Beckmann Coulter, Germany

Water bath, GFL, Germany

Microplate Reader Spark®, Tecan, Switzerland

Multimode Plate Reader EnSpire® 2300, PerkinElmer, USA

96-well black plates, Thermo Fisher Scientific, USA

OP96U OxoPlates®, PreSens Precision Sensing GmbH, Germany

Cell Culture Flasks 25 cm^2, Greiner bio-one, Germany

Cell Culture Flasks 75 cm^2, Greiner bio-one, Germany

Reagent reservoir Dual Solution®, VWR, USA

15 mL Cellstar® Tube, Greiner bio-one, Germany

50 mL Cellstar® Tube, Greiner bio-one, Germany

30 mL PP Universal Container, Thermo Fisher Scientific, USA

Reaction Tubes 1 mL PP, Greiner bio-one, Germany

Reaction Tubes 2 mL PP, Greiner bio-one, Germany

Eppendorf Tubes®, 5 mL, Eppendorf, Germany

Pipettes, Gilson, USA

Pipettes, Eppendorf, Germany

Pipette tips, Greiner bio-one, Germany

Pipetus® standard, Hirschmann Laborgeräte, Germany

Eppendorf research plus pipette, Eppendorf, Germany

epT.I.P.S.® - Pipette tips, Eppendorf, Germany

Multipette® M4, Eppendorf, Germany

Combitips advanced®, Eppendorf, Germany

Examination gloves, Hartmann, Germany

2.1.3 Chemicals

Dulbecco's Modified Eagle's Medium (DMEM)- high glucose, Sigma-Aldrich, Germany

Colourless Dulbecco's Modified Eagle's Medium (DMEM)- high glucose, Sigma-Aldrich, Germany

Foetal bovine serum, Sigma-Aldrich, Germany

B27 supplement minus AO, Invitrogen, UK

Sodium Pyruvate solution, Sigma-Aldrich, Germany

L-Glutamine, Sigma-Aldrich, Germany

Trypan blue, Sigma-Aldrich, Germany

Dulbecco's Phosphate Buffered Saline + pyruvate and glucose, Thermo Fisher Scientific, USA

Dulbecco's Phosphate Buffered Saline 10x, Thermo Fisher Scientific, USA

Sodium sulfite, anhydrous, Merck, Germany

Paraffin oil viscid puriss, Sigma-Aldrich, Gemany

5,5′,6,6′-Tetrachloro-1,1′,3,3′-tetraethyl-imidacarbocyanine iodide (JC-1), Abcam, GB

Poly-D-lysine hydrobromide (PDL), Sigma-Aldrich, Germany

Dimethyl sulfoxide (DMSO), Merck, Germany

Rotenone, Sigma-Aldrich, Germany

Carbonyl cyanide-3-chlorophenylhydrazoe, Sigma-Aldrich, Germany

Oligomycin from Streptomyces, Sigma-Aldrich, Germany

Δ^9-Tetrahydrocannabinol, Weltapotheke, Austria

2.2 Methods

2.2.1 Neuroblastoma Cell Line

The murine neuroblastoma cells N18TG2 (purchased from German Collection of Microorganisms and Cell Cultures, Germany) were maintained in Dulbecco's Modified Eagle's medium (DMEM), containing phenol red as a pH-indicator. The medium was supplemented with 10 % fetal calf serum (FBS, Sigma-Aldrich, Germany), 2 mM L-glutamine (Sigma-Aldrich, Germany) and 2 mM sodium pyruvate (Sigma-Aldrich, Germany). Cells were maintained in 25 cm^2 and 75 cm^2 cell culture flasks (Greiner bio-one, Germany) and split when 80 % confluent. Cells were kept in a humidified incubator at 37 °C, with 5 % CO_2.

2.2.2 Cell Culture Treatment

Solutions of mitochondrial modulators were prepared in dimethyl sulfoxide (DMSO; Merck, Germany) and diluted in Dulbecco's Phosphate Buffered Saline with added pyruvate and glucose (Thermo Fisher Scientific, USA). In each dilution as well as in the vehicle control the DMSO concentration was equivalent. The DMSO concentration of the highest concentrated inhibitor solution that was used in experiments defined the concentration of DMSO used in the dilutions. All other solutions were also prepared and washing steps were performed using Dulbecco's Phosphate Buffered Saline with pyruvate and glucose, which will be referred to as PBS for simplicity.

For the freshly prepared rotenone (Sigma-Aldrich, Germany) solutions, rotenone was weight and dissolved in DMSO to obtain a 10 mM stock solution before every experiment. The stock was diluted to receive the following in-well concentrations: 160 nM, 80 nM, 40 nM, 20 nM, 10 µM, 5 µM, and 2.5 µM. The rotenone control well contained 0.000016 % of DMSO.

CCCP (Sigma-Aldrich, Germany) treatment was performed using a 50 mM stock solution (10.231 mg/mL DMSO, kept at -20 °C). The stock was diluted to obtain the following in-well concentrations: 100 µM, 50 µM, 10 µM, 5 µM, 1 µM, 0.5 µM, and 0.25 µM. The control well of CCCP contained 0.2 % of DMSO.

For Oligomycin (Sigma-Aldrich, Germany), a 3 mM DMSO-stock was used (2.373 mg/mL DMSO, kept at -20 °C) to obtain in-well concentrations of 3 µM, 2 µM, 1 µM, 0.5 µM, 0.25 µM and 0.1 µM. All wells, including the vehicle control, contained 0.1 % of DMSO.

Cells were treated with the final concentration of 10 µM of THC (Weltapotheke, Austria). The 25 mM THC DMSO-stock (7,862 mg/mL, dissolved in DMSO, stored at -20 °C) was diluted with PBS. Vehicle controls were prepared with PBS containing the same amount of DMSO. Cells were incubated for four hours at 37° C and 5 % CO_2 prior to the experiments.

2.2.3 Measurement of the Mitochondrial Membrane Potential with JC-1

5,5′,6,6′-Tetrachloro-1,1′,3,3′-Tetraethyl-imidazolocarbocyanine Iodide (JC-1, Abcam, GB) is a lipophilic, cationic, carbocyanine dye. It selectively accumulates in mitochondria, due to the electrochemical gradient from the MMP and forms complexes subjective to its concentration. JC-1 exhibits green fluorescence emission (measurable at 535nm) as a monomer at low concentrations, whereas the dimer emits red fluorescence emission (measurable at 590 nm) when JC-1 concentration is high. The excitation wavelength used for both dyes was 280 nm. The MMP is assessed by the ratio of red to green, the red/green ratio is up following a hyperpolarized MMP.

Cells were seeded on precoated black 96-well plates (Thermo Fisher Scientific, USA). The day before treatment, 50 µL per well of a 100 µg/mL poly-D-lysin hydrobromide (PDL, Sigma-Aldrich, Germany) solution was pipetted on the plate and incubated for 24 hours at 37 °C. For measurements, the cell medium was switched to colorless DMEM containing 2% B-27 (Invitrogen, UK), 2 mM L-glutamine and 2 mM sodium pyruvate. 5 mL of the medium was used to wash down the adherent cells and generate a cell suspension. Cells were then counted using a hemocytometer (Bartelt, Austria). Therefore, the cell suspension was 1:5 diluted with PBS and an equal amount of trypan blue (Sigma-Aldrich, Germany) was added. Cells of four corner squares were counted. The cell suspension was diluted to a concentration of 400,000 cells/mL. After removing the PDL solution and washing the wells with PBS, 150 µL of cell suspension was added. Plates were incubated for 24 hours to enable the cells to grow

onto the plate. JC-1 was added to the whole plate to reach a final in-well concentration of 3.06 µM. Plates were incubated for 30 minutes at 37 °C and washed two times with 90 µL PBS. 90 µL PBS was again added to each well and incubated for an additional 15 minutes in the incubator at 37 °C to establish an equilibrium state. A first measurement of all wells was done and used to determine the relative change of the MMP. Induction of changes in the MMP by mitochondrial modulators was performed by adding a tenth of the well volume of inhibitory substances or controls. Measurements were performed using the microplate reader Spark® (Tecan, Switzerland). Changes in the MMP were observed over 20 minutes for the inhibitor experiments, cannabinoid treatment was observed over 25 minutes. The red/green ratio was calculated for every well. To account for the decay of the green JC-1 monomer, that happens upon the dye's excitation, the bleaching factor was determined for every row of the plate for every measurement, except the first one. The bleaching factor was calculated by dividing the former measurement of the control well by its current one. Every well of the row was then multiplied with the bleaching factor. The first measurement (without inhibitor treatment) of all wells was set to 100% and the relative change of the MMP was calculated for the following timepoints.

2.2.4 Measurement of the Oxygen Consumption with OxoPlates®

The OxoPlate® OP96U (PreSens, Germany) is a 96-well multiplate containing an oxygen sensor, a polymer film with two covalently bound dyes, at the bottom of every well. While the intensity of the indicator dye (emission is detected at 650 nm) correlates to the oxygen concentration in the well, the reference dye (emission is measured at 590 nm) is independent of the oxygen content; the excitation wavelength is 540 nm for both dyes. The ratio of dyes is calculated to assess the oxygen content normalized to the sensor response.

In accordance with the manufacturer instructions, measurements were calibrated using air-saturated PBS (kept on a magnetic stirrer for at least 12 hours at room temperature), serving as the air-saturated solution and referred to as 100 % relative oxygen concentration. For the oxygen-free solution, double distilled water was saturated with sodium sulfite (Na_2SO_3, Merck, Germany). Inhibitor solutions and controls (10 % of the final well-volume) were applied to the

plate at least 30 minutes before the measurement to ensure the equilibration of the sensor. Cells were resuspended from the cell flasks with their normal medium. Cells were counted using a hemocytometer (Bartelt, Austria). The cell suspension was 1:5 diluted with PBS and an equal amount of trypan blue (Sigma-Aldrich, Germany) was added. Cells of four corner squares were counted. The volume of the cell suspension equal to 4,000,000 cell was moved to a Cellstar® Tube (Greiner bio-one, Germany) and centrifuged at 650 g for five minutes. The cell pellet was then resuspended using 1 mL of the air-saturated PBS. 90 µL of the air-saturated PBS and 50 µL of the cell suspension were added. All wells, including the wells containing the air-saturated and oxygen-free solutions (respectively 150 µL), were covered immediately with 100 µL paraffin oil (Sigma-Aldrich, Germany) after all components were included. Measurements were conducted using the multimode plate reader EnSpire® 2300 (PerkinElmer, USA), which measured the plate from below. Wells were observed for 35 minutes. Measurements were calibrated using the solution with 100 % relative oxygen concentration (k_{100}) and the oxygen-free solution (k_0). The following formula was used to calculate the oxygen content of wells, I_R represents the ratio of the indicator dye to the reference dye:

$$pO_2 = 100\ x \left(\frac{k_0}{I_R} - 1\right) / \left(\frac{k_0}{k_{100}} - 1\right)$$

2.2.5 Statistical Analysis

For the treatment with different mitochondrial function modulators, data were obtained from six independent experiments; only the measurement of the oligomycin-treated OxoPlate® was repeated eight times. Samples at different treatment conditions were measured in duplicates.

Replicates of the experiments with THC-treated cells were done five times, also independently from each other. Inhibitory solutions were applied in quadruplicates for JC-1 and duplicates for the OxoPlate® measurements.

Statistical analysis was done using a Kruskal-Wallis (H)-test followed by a Chi^2-test (displayed as *). To determine significant differences between two groups, a Mann-Whitney U-test was performed (displayed as #). Significance was accepted when p-values remained under 0.05.

3 Results

3.1 Determination of Effective Concentrations of Mitochondrial Modulators

The three ETC operation modulators rotenone, CCCP, and oligomycin were diluted to determine an effective concentration of every modulator that provoked a specific reaction in the cells. Samples were observed for a change in the MMP by measuring and calculating the red/green ratio of JC-1, and their oxygen consumption was assessed through the OxoPlate®.

3.1.1 Concentration-dependent Effect of Rotenone-induced Toxicity

Rotenone-induced toxicity did not lead to significant changes in the MMP in any concentration, as demonstrated by the JC-1 data. Although it was not significant, a slight increase in the red/green ratio (hyperpolarization) was observed in all concentrations upon the addition of the inhibitor.

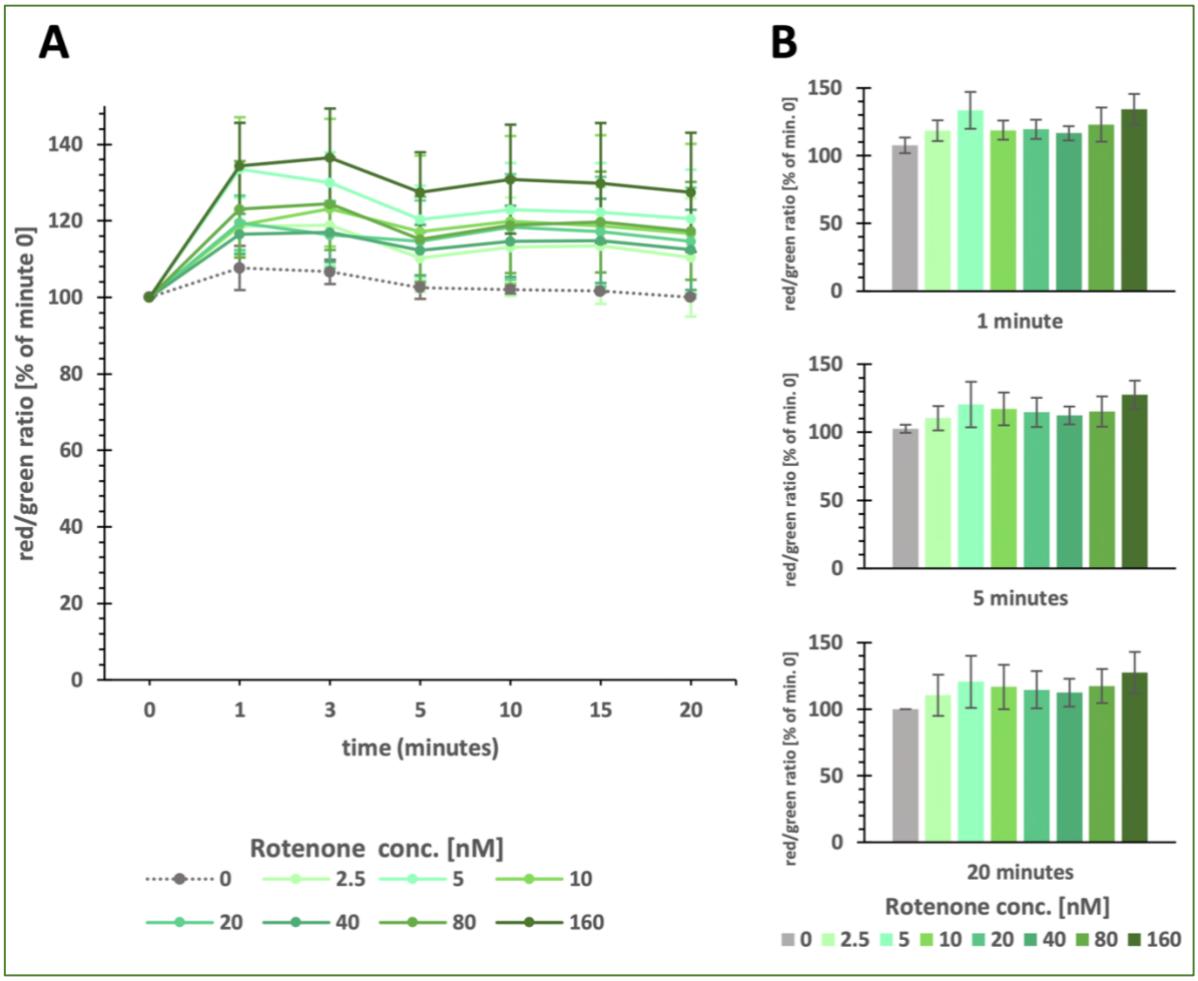

Figure 10: JC-1 measurements of the concentration-dependent effect of rotenone
(**A**) Lines display the MMP of cells treated with rotenone for different time points. (**B**) Bar charts display the influence of rotenone concentrations at specific time points.
No statistical significance was found using the Kruskal-Wallis (H)-test followed by the Chi^2-test ($p < 0.05$). Displayed is the mean +/- the standard error of the mean of three independent experiments

Rotenone led to a significant decrease in the oxygen consumption at a 160 nM concentration. The oxygen consumption almost entirely stopped 10 minutes after the addition of the inhibitor, and oxygen content stayed at about 85 %. Lower concentrations of rotenone (e.g., 2.5 nM, 5 nM, and 10 nM) had essentially the same oxygen consumption as the control. Rotenone decreased the oxygen consumption at a concentration of 20–80 nM, but those changes were not significant.

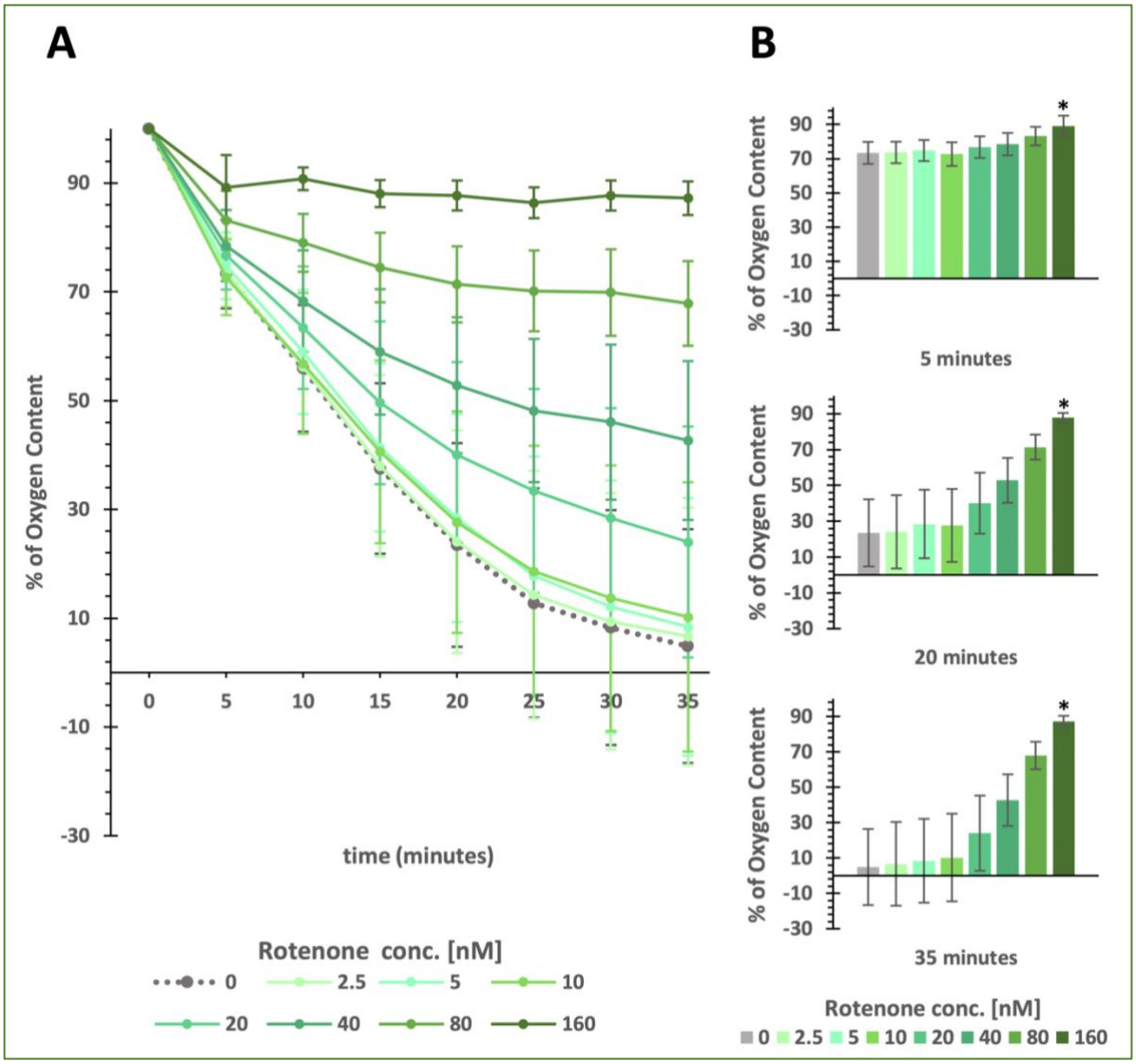

Figure 11: OxoPlate® measurements of the concentration-dependent effect of rotenone
(**A**) Lines display the oxygen content of wells treated with rotenone for different time points. (**B**) Bar charts display the influence of rotenone concentrations at specific time points.
Statistical significance was determined with the Kruskal-Wallis (H)-test followed by the Chi^2-test ($p < 0.05$) and is displayed as (*). Displayed is the mean +/- the standard error of the mean of five independent experiments

Subsequently, the 160 nM in-well concentration was used for the THC experiments.

3.1.2 Concentration-dependent Effect of CCCP-induced Toxicity

CCCP led to a significant decrease in the red/green ratio at an in-well concentration of 1 µM, 20 minutes after the addition of the inhibitor. A significant depolarization of the MMP (decrease in the red/green ratio) was also observed for 0.025 µM wells starting at 15 minutes after the inhibitor treatment, leading to a decrease in the red/green ratio of about 10 %.

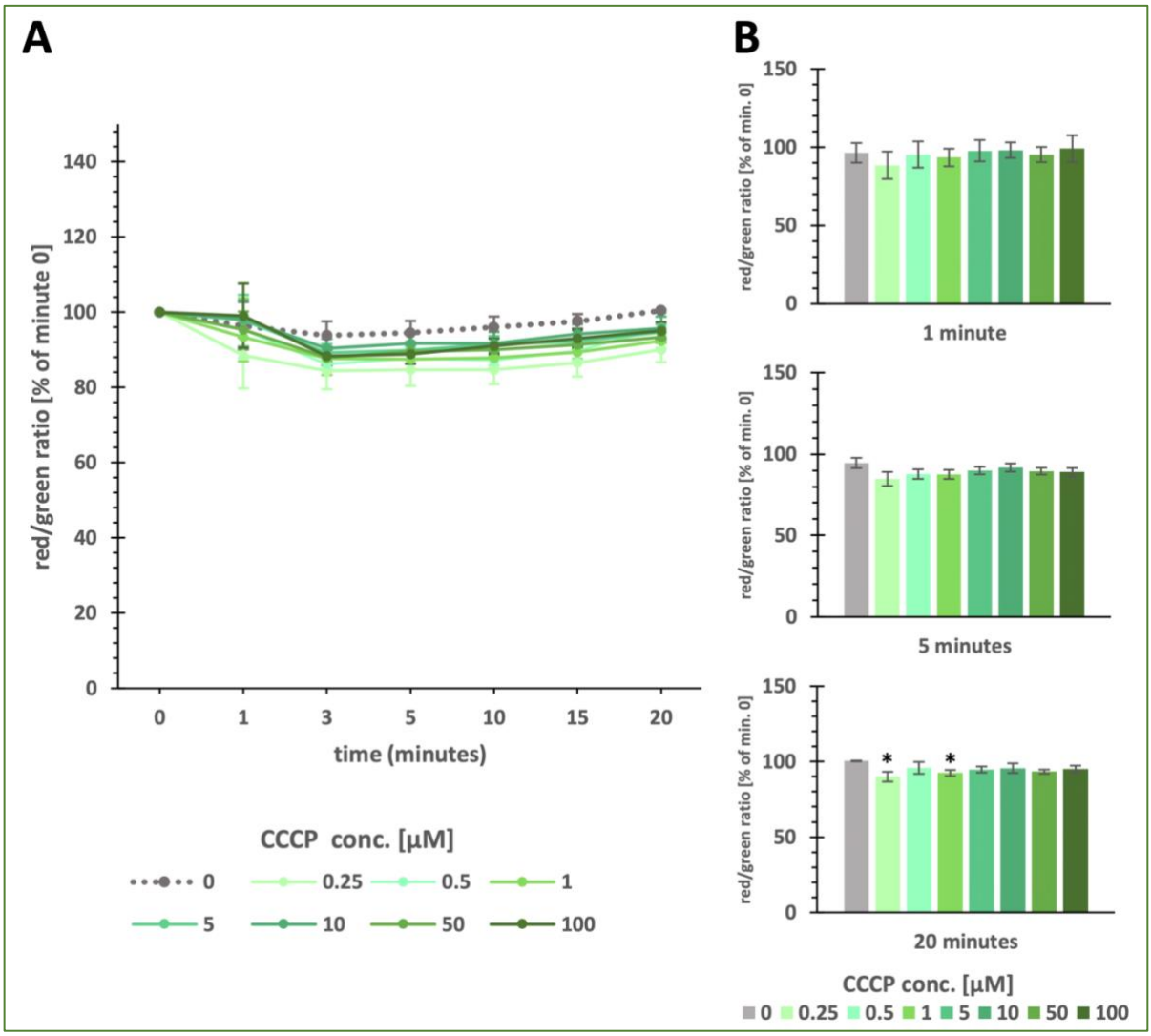

Figure 12: JC-1 measurements of the concentration-dependent effect of CCCP
(**A**) Lines display the MMP of cells treated with CCCP for different time points. (**B**) Bar charts display the influence of CCCP concentrations at specific time points.
Statistical significance was determined with the Kruskal-Wallis (H)-test followed by the Chi^2-test ($p < 0.05$) and is displayed as (*). Displayed is the mean +/- the standard error of the mean of six independent experiments

Lower concentrations of CCCP, such as 10 µM, 5 µM and 1 µM, led to a significantly accelerated oxygen consumption and led to in-well oxygen contents of 0 %, in some cases even under 0 %. In higher concentrations, such as 100 µM and 50 µM, CCCP reduced the oxygen consumption, although these findings were not significant. Concentrations under 1 µM did not significantly differ from the control, although a decrease in the oxygen content was observed.

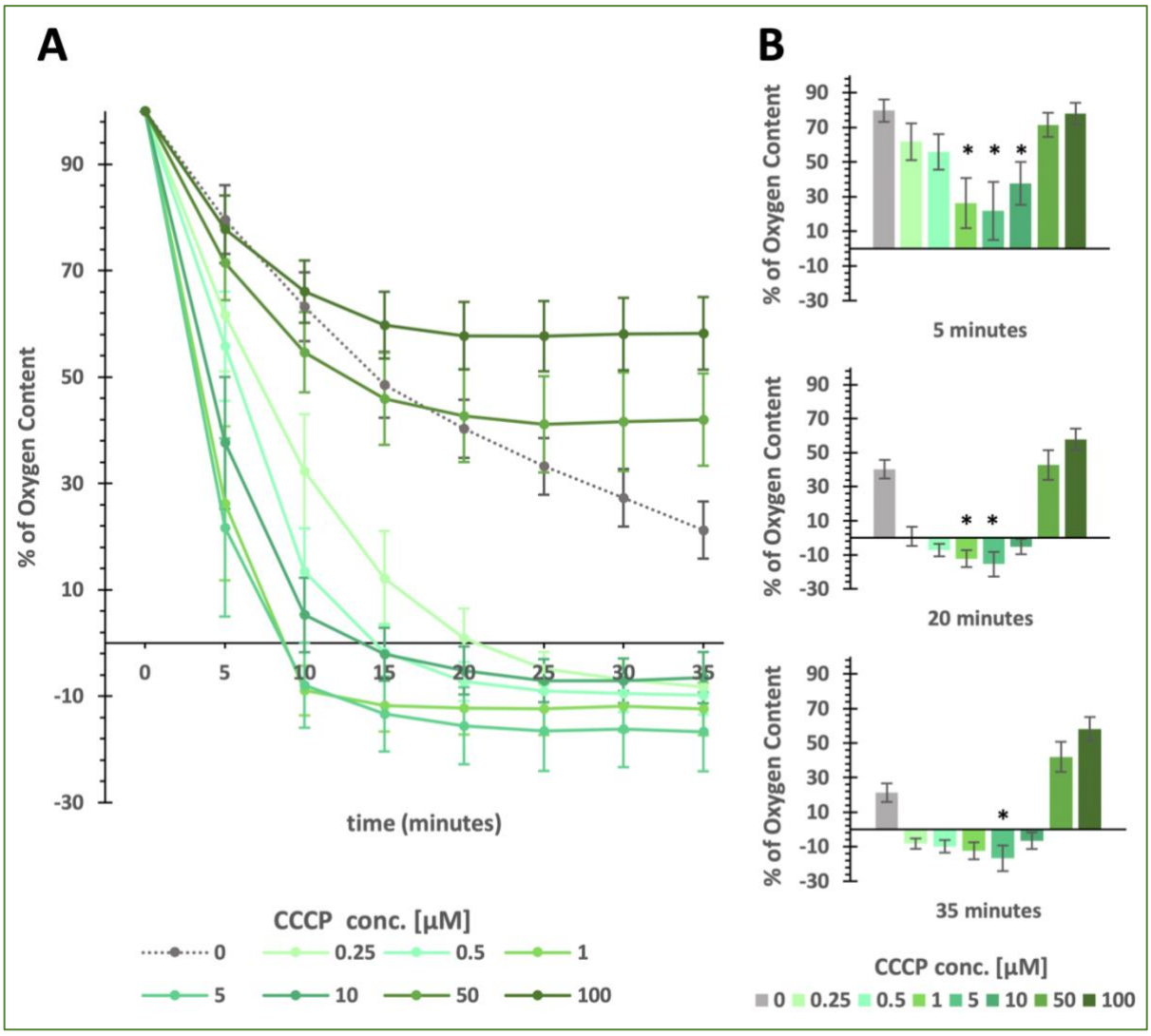

Figure 13: OxoPlate® measurements of the concentration-dependent effect of CCCP
(**A**) Lines display the oxygen content of wells treated with CCCP concentrations for different time points. (**B**) Bar charts display the influence of CCCP concentrations at specific time points. Statistical significance was determined with the Kruskal-Wallis (H)-test followed by the Chi^2-test ($p < 0.05$) and is displayed as (*). Displayed is the mean +/- the standard error of the mean of six independent experiments

The 1 µM in-well concentration was then used for the experiments with THC-treated cells.

3.1.3 Concentration-dependent Impact of Oligomycin-induced Toxicity

JC-1 measurements did not reveal any significant differences in the MMP for oligomycin treatment. In-well concentrations of 3 µM led to a mean increase of over 10 % in the red/green ratio, although this increase was not significant. The red/green ratios of other concentrations were close to the control, with variances under 10 %.

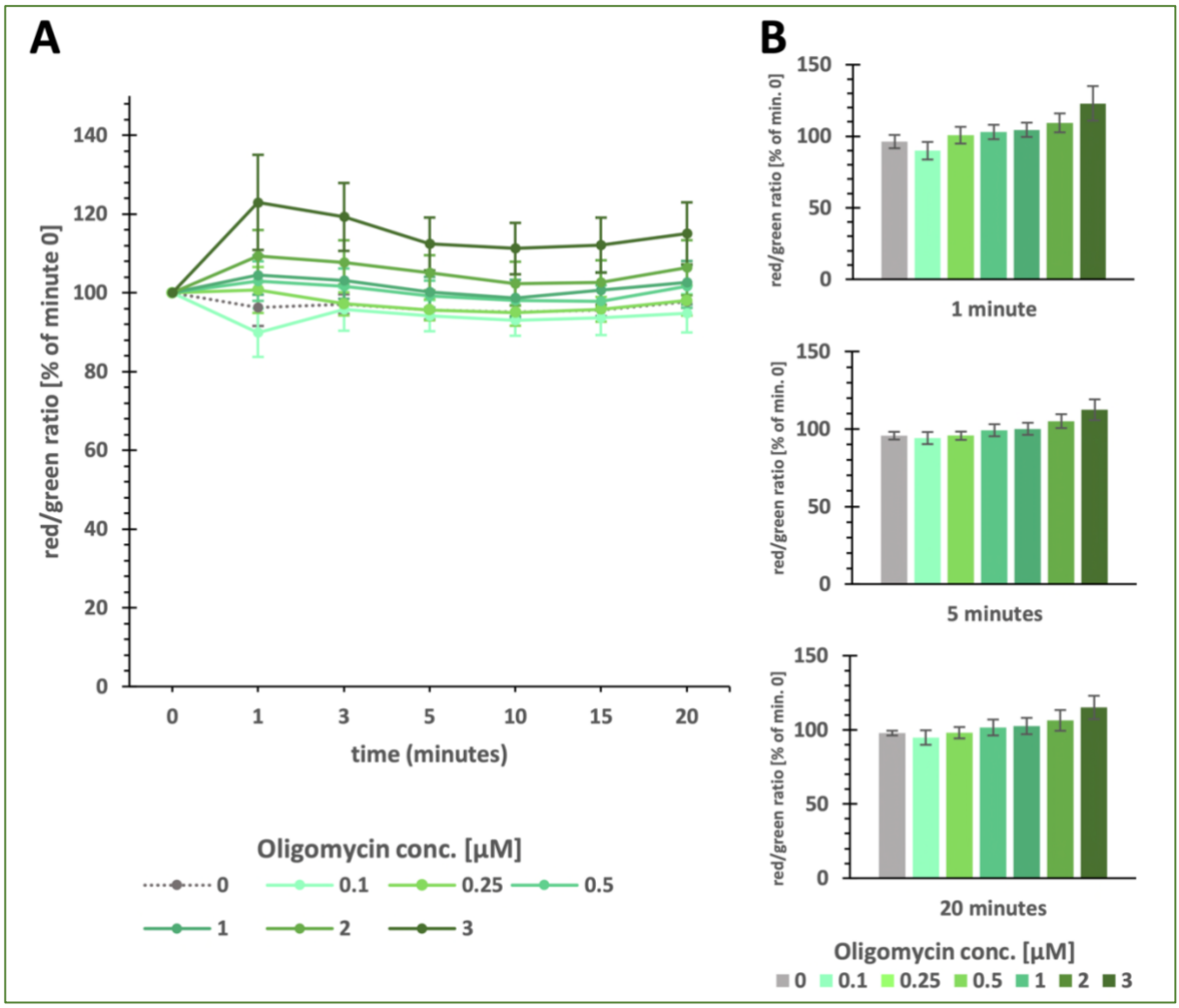

Figure 14: JC-1 measurements of the concentration-dependent effect of oligomycin
(**A**) Lines display the MMP of cells treated with oligomycin for different time points. (**B**) Bar charts display the influence of oligomycin concentrations at specific time points.
No statistical significance was found using the Kruskal-Wallis (H)-test followed by the Chi^2-test ($p < 0.05$). Displayed is the mean +/- the standard error of the mean of six independent experiments

The oxygen consumption of all concentrations of oligomycin was almost identical to the control. No significant differences were observed.

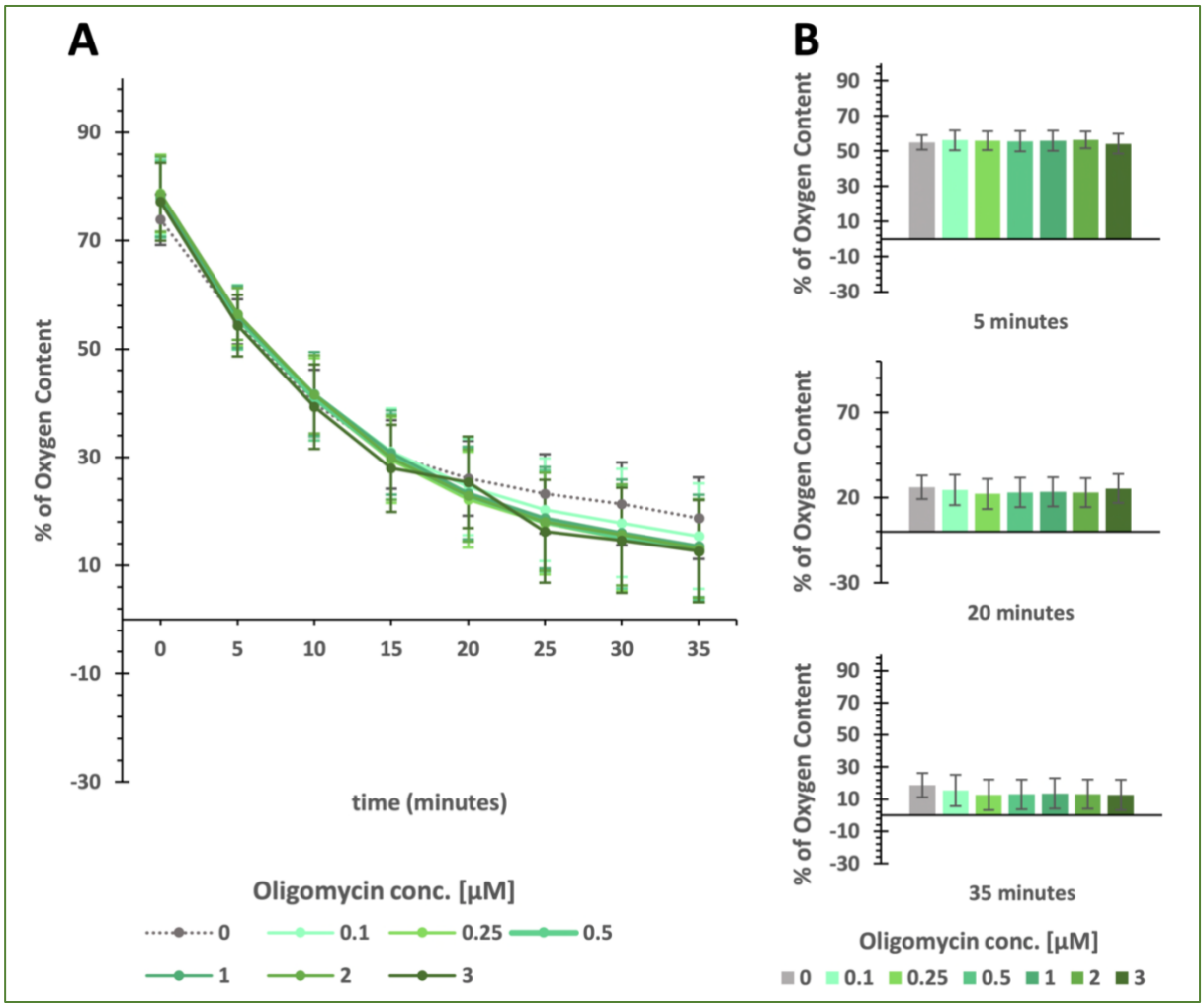

Figure 15: OxoPlate® measurements of the concentration-dependent effect of oligomycin
(**A**) Lines display the oxygen content of wells treated with different concentrations of oligomycin.
(**B**) Bar charts display the influence of oligomycin concentrations at specific time points.
No statistical significance was found using the Kruskal-Wallis (H)-test followed by the Chi^2-test ($p < 0.05$). Displayed is the mean +/- the standard error of the mean of eight independent experiments

Due to no observed significant differences, no oligomycin concentration was used for the THC experiments.

3.2 Effects of THC

Cells were treated with THC (or the control solution) and observed for changes in their reaction to the selected concentrations of the mitochondrial modulators rotenone and CCCP. Changes in the MMP and oxygen consumption were observed four hours afterward. The addition of the modulators and conduction of the experiments was carried out in the same manner as it was done for the determination of effective concentrations of modulators of the ETC. Because a single measurement of the JC-1 plate took five minutes (more wells were measured than in the determination of effective concentrations experiments), the MMP could only be observed directly after adding the modulators and then again after five minutes.

Evaluation of the red/green ratio of JC-1 measurements revealed differences in the MMP between THC-treated and untreated cells before the inhibitor addition. THC treatment significantly decreased the red/green ratio to about 94 % of the control. Because this study wanted to observe the differences in the effects of modulators on treated and untreated cells, the measurement of every well before the inhibitor was added was set to 100 % for JC-1 measurements.

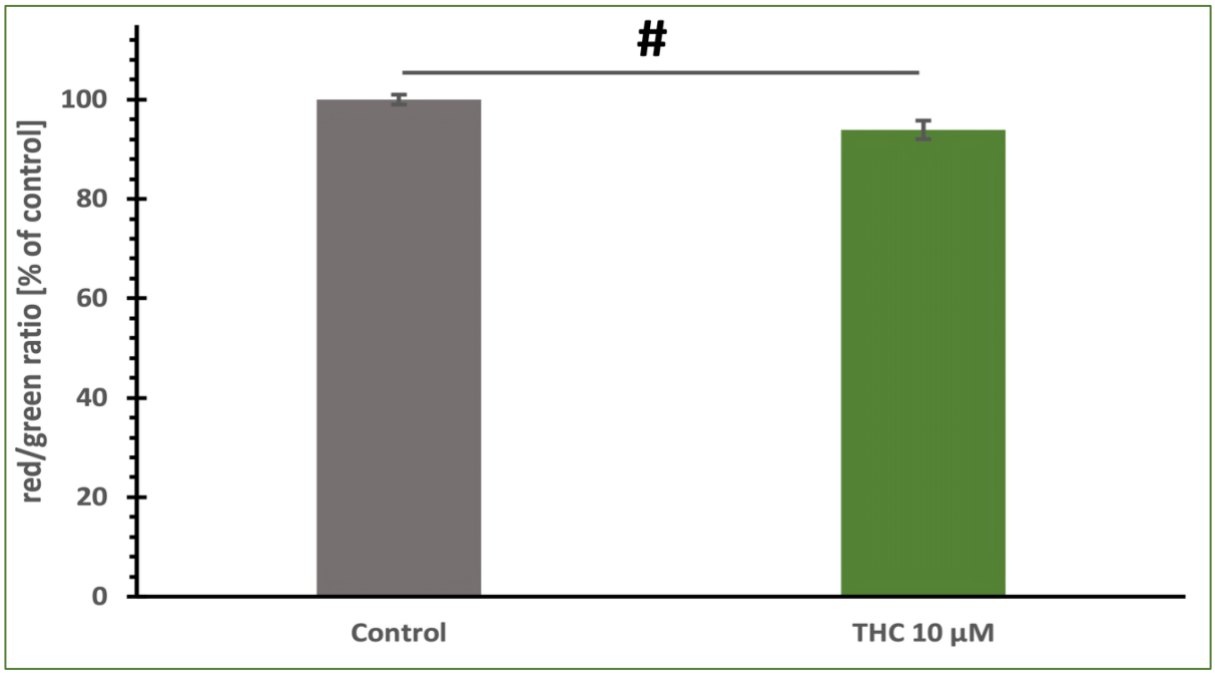

Figure 16: Comparison of the MMP
Comparison of untreated control cells and cells treated for four hours with 10 µM of THC. Statistical significance was determined with the Mann-Whitney U-test ($p < 0.05$) and is displayed as (#). Displayed is the mean +/- the standard error of the mean of four independent experiments

3.2.1 Effects of THC in Cells with Rotenone-induced Toxicity

In THC-treated cells, a slight and significant increase in the red/green ratio of approximately 5 % was observed. No significant changes in the MMP were observed upon the addition of the 1.6 µM of rotenone in control cells and it was almost identical to the MMP of cells that received the rotenone-free control solution.

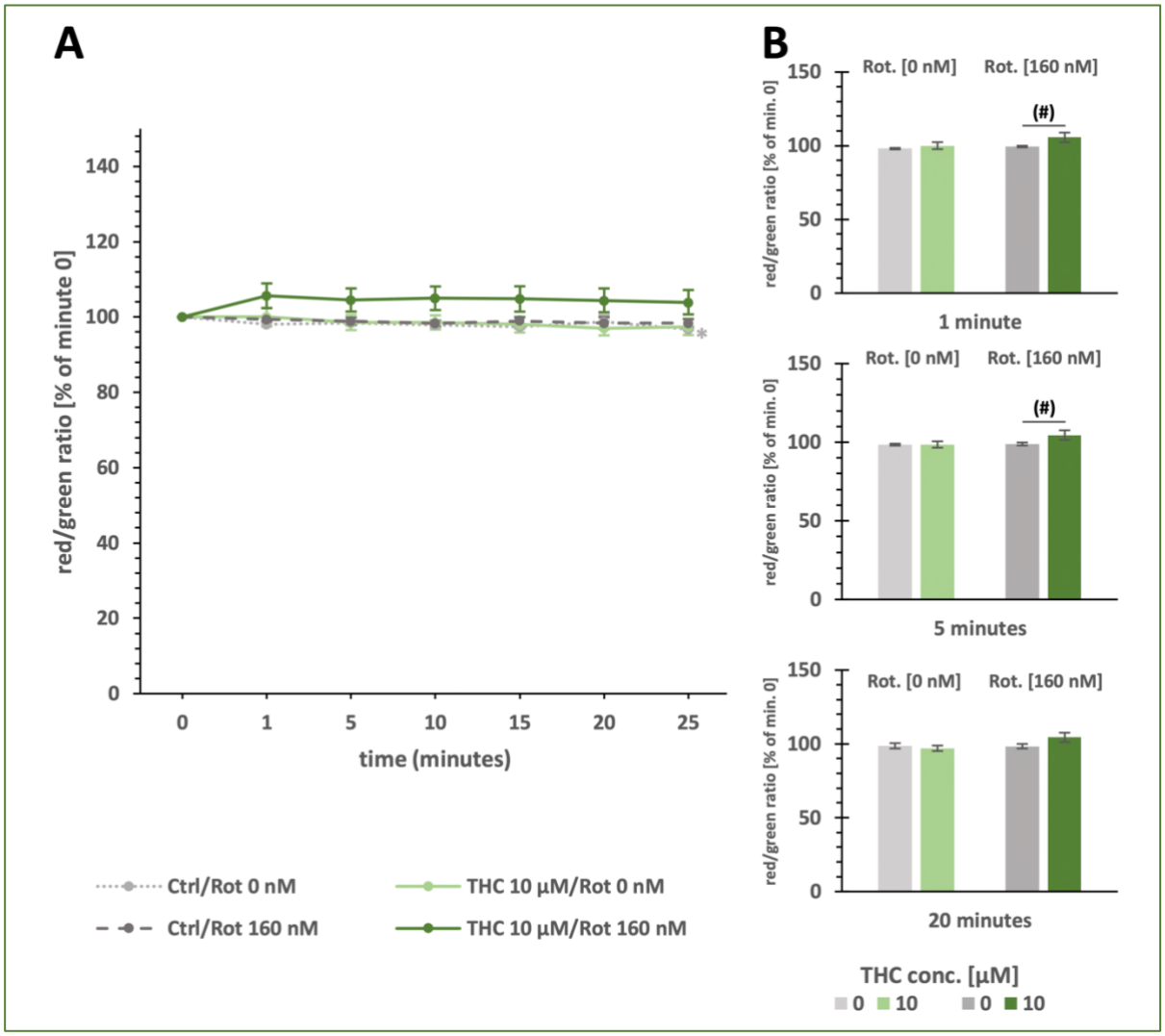

Figure 17: JC-1 measurements of the effects of THC on rotenone-induced toxicity
(**A**) Lines display the MMP of cells treated with THC and/or rotenone. (**B**) Bar charts display the influence of THC and rotenone on the MMP at specific time points.
Statistical significance was determined with the Kruskal-Wallis (H)-test followed by the Chi^2-test (displayed as *) and the Mann-Whitney U-test (displayed as #) ($p < 0.05$). Displayed is the mean +/- the standard error of the mean of five independent experiments. An effect of THC on rotenone-induced toxcitiy was observed, but inspection of the data revealed that it was only present in one experiment

THC did not significantly affect the oxygen consumption of cells, independent of rotenone treatment. The rotenone-induced significant decrease in oxygen consumption was observed in cells treated with THC and untreated control cells. At a 160 nM in-well concentration of rotenone oxygen content remained at about 70 % for both. Wells with no added rotenone consumed more oxygen and decreased the content to about 35 %.

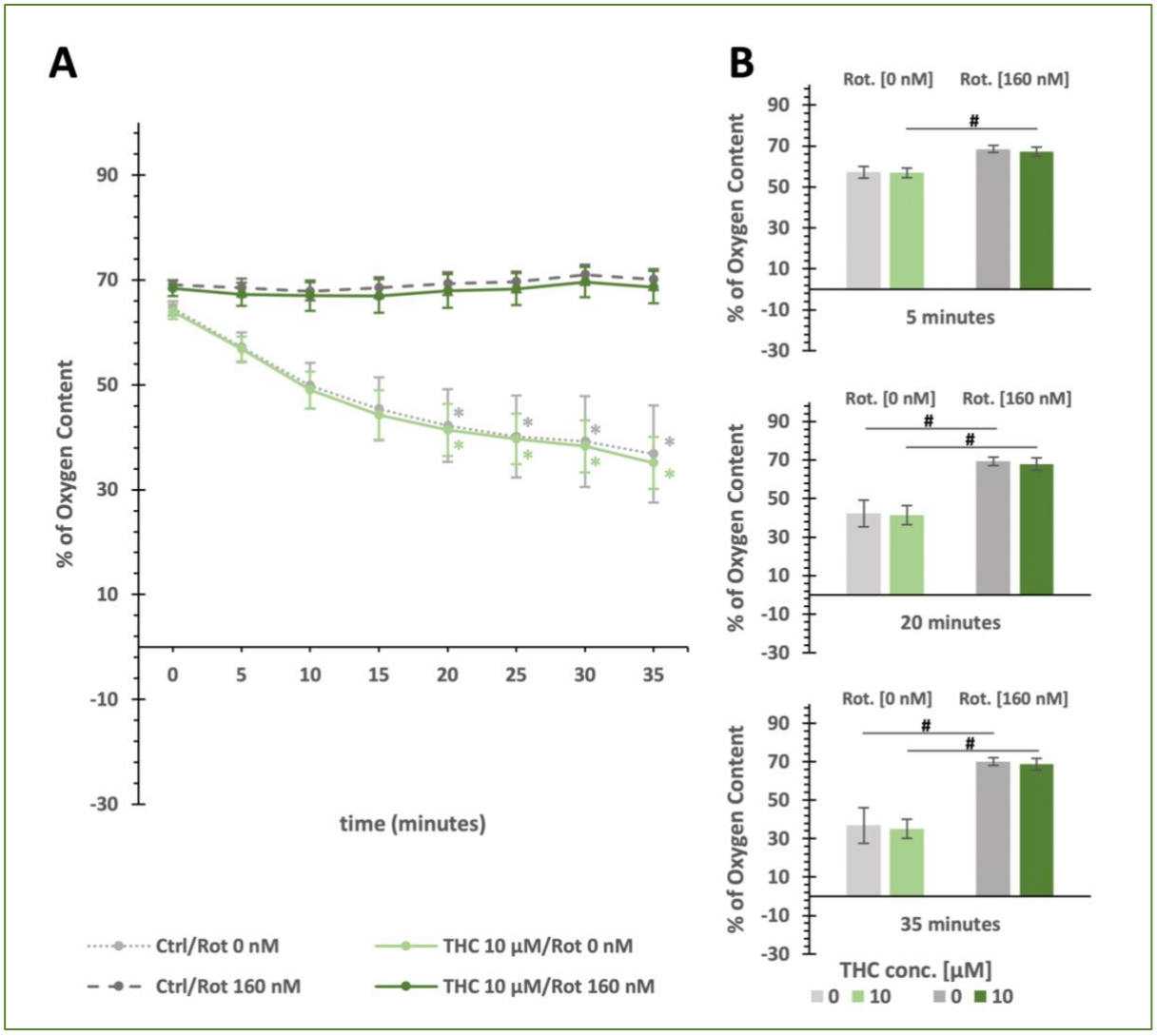

Figure 18: OxoPlate® measurements of the effects of THC on rotenone-induced toxicity
(**A**) Lines display the oxygen content of wells treated with THC and/or rotenone. (**B**) Bar charts display the influence of THC and rotenone on the oxygen content at specific time points.
Statistical significance was determined with the Kruskal-Wallis (H)-test followed by the Chi^2-test (displayed as *) and the Mann-Whitney U-test (displayed as #) ($p < 0.05$). Displayed is the mean +/- the standard error of the mean of five independent experiments

3.2.2 Effects of THC in Cells with CCCP-induced Toxicity

CCCP treatment led to a mean decrease of 30 % in the red/green ratio immediately after adding the inhibitor (1 µM in-well concentration). This was observed in THC-treated and control cells. The red/green ratio was unchanged at 70% for the remaining time of the measurement. No significant differences were observed between the cell types. The MMP of cells treated with the control solution did not change significantly.

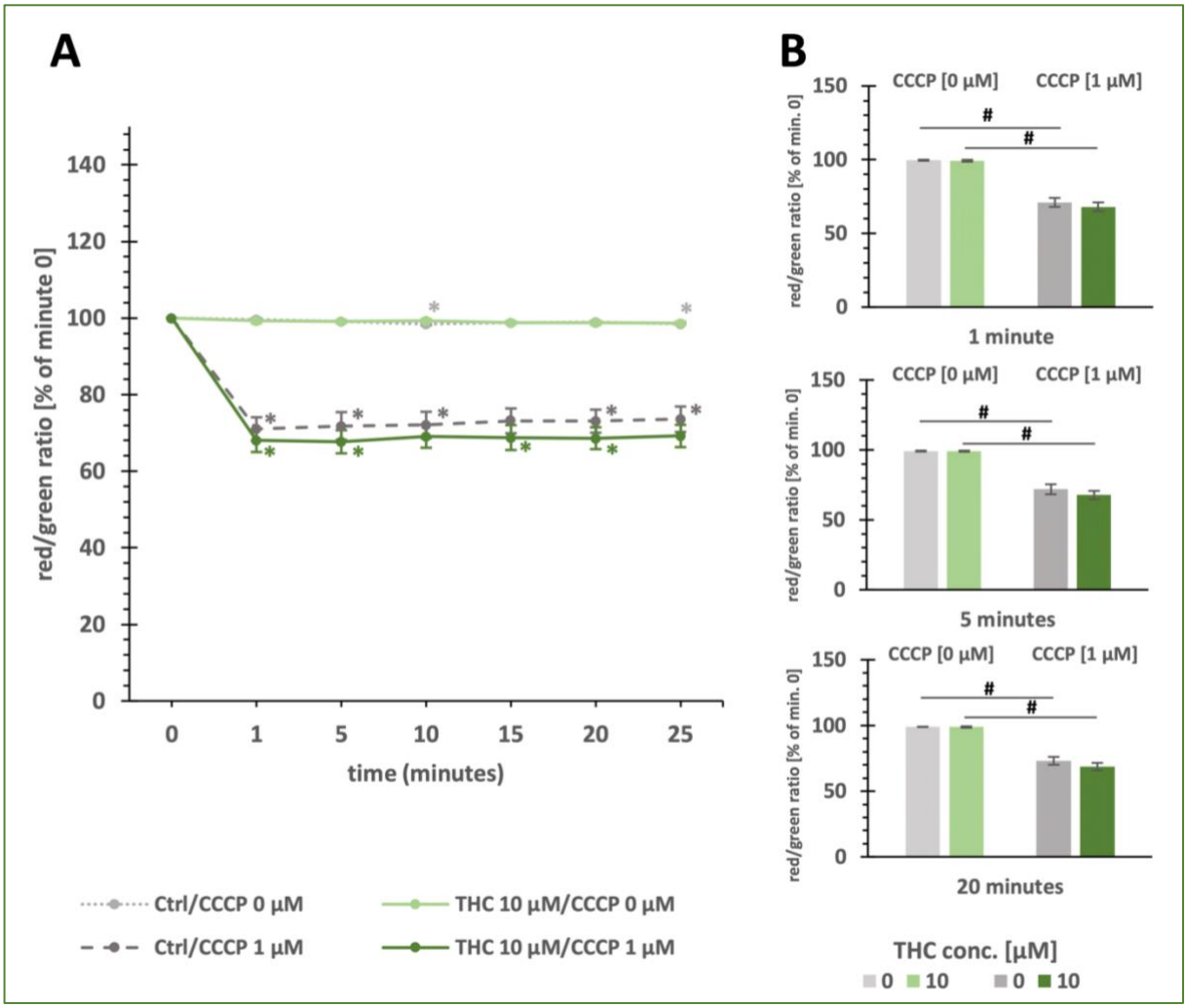

Figure 19: JC-1 measurements of the effects of THC on CCCP-induced toxicity
(**A**) Lines display the MMP of cells treated with THC and/or CCCP. (**B**) Bar charts display the influence of THC and CCCP on the MMP at specific time points.
Statistical significance was determined with the Kruskal-Wallis (H)-test followed by the Chi^2-test (displayed as *) and the Mann-Whitney U-test (displayed as #) ($p < 0.05$). Displayed is the mean +/- the standard error of the mean of five independent experiments

The acceleration of the oxygen consumption followed the addition of the inhibitor CCCP. Notably, THC-treated cells that received CCCP treatment did have a significantly different oxygen consumption from the beginning. The effect in control cells of 1 µM CCCP was only significant after 15 minutes. Wells without CCCP decreased the oxygen content to 30–35 %, while wells containing 1 µM of CCCP decreased it to under 10 %.

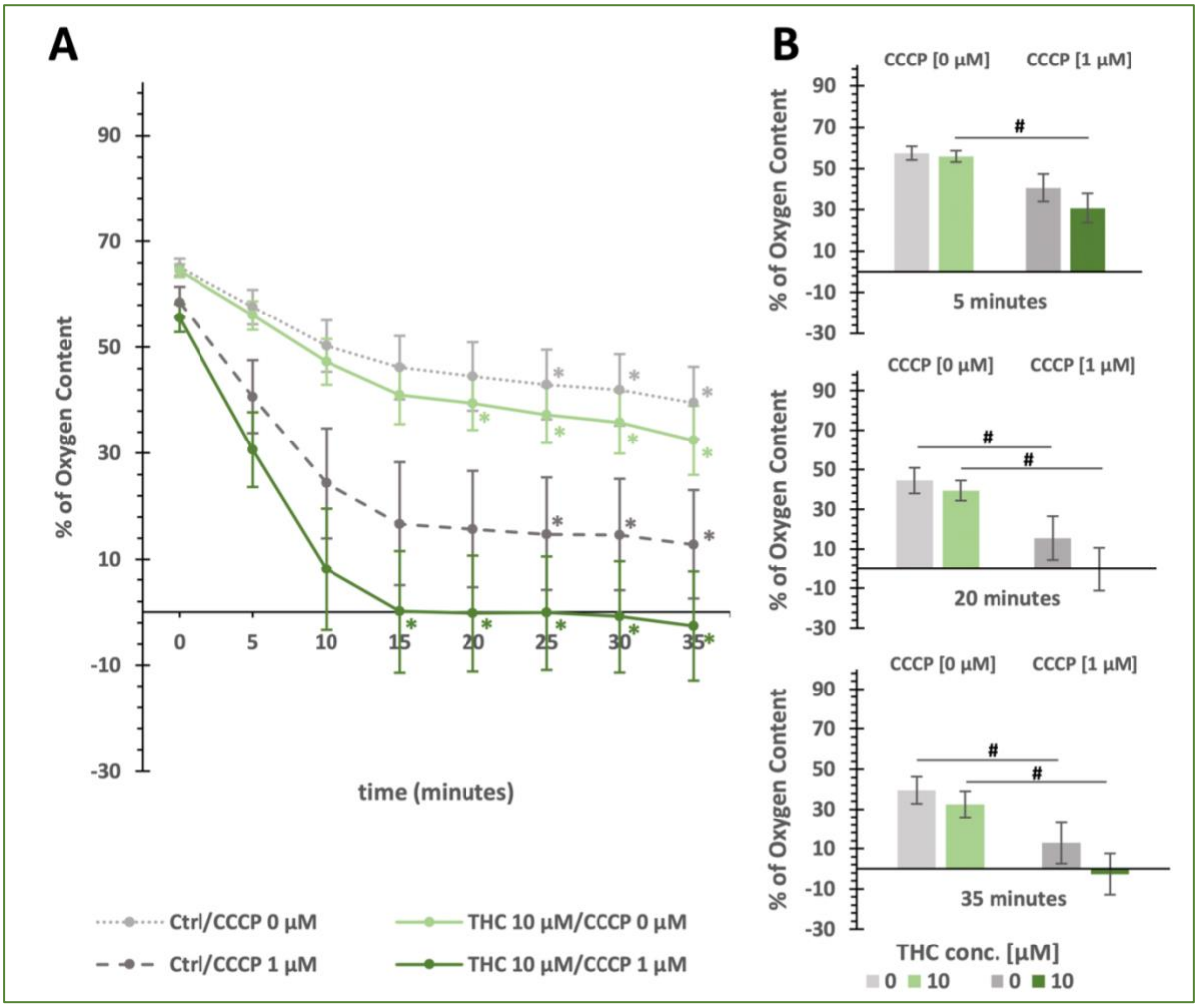

Figure 20: OxoPlate® measurements of the effects of THC on CCCP-induced toxicity
(**A**) Lines display the oxygen content of wells treated with THC and/or CCCP. (**B**) Bar charts display the influence of THC and CCCP on the oxygen content at specific time points.
Statistical significance was determined with the Kruskal-Wallis (H)-test followed by the Chi^2-test (displayed as *) and the Mann-Whitney U-test (displayed as #) ($p < 0.05$). Displayed is the mean +/- the standard error of the mean of five independent experiments

4 Discussion

4.1 Concentrations of the tested mitochondrial toxins

4.1.1 Influence of Rotenone Inhibition

Rotenone has been shown to depolarize the MMP *in vitro* when rotenone treatment occurred several hours before the experiments were conducted (Moon et al., 2005). Other studies found a slight hyperpolarization of the MMP, as determined by flow cytometry after 20 minutes (Tada-Oikawa et al., 2003; Won et al., 2015). Therefore it is hypothesized that the formation of ROS, induced by rotenone treatment, is responsible for the MMP depolarization (Tada-Oikawa et al., 2003). In this study, no significant difference in the MMP was observed upon rotenone treatment, although a slight increase in the red/green ratio was observed through all concentrations. This tendency of the cells to react to rotenone treatment with a MMP hyperpolarization contrasts data previously obtained by the institute after 48 hours (Radad et al., 2006). The current literature does not provide data on this issue. This slight hyperpolarization of the MMP shortly after the addition of the inhibitor suggests that the depolarization of the MMP might be a secondary effect of the rotenone treatment that only occurs after several hours.

The concentration-dependent inhibition of the oxygen consumption by rotenone was previously reported and linked to the activity of complex I (Li et al., 2003; Telford et al., 2009). Rotenone stopped the oxygen consumption almost entirely at higher concentrations, while lower concentrations did not significantly affect it and only decreased it to a lower extent. These findings were according to the literature (Telford et al., 2009).

The findings suggest that at a 160 µM concentration, rotenone inhibits complex I almost immediately, as shown by the stop of the oxygen consumption. Significant changes in the MMP were not observed at any concentration and propose a slow MMP depolarization. Therefore, the 160 µM concentration was used for the THC experiments.

4.1.2 Influence of CCCP Modulation

As expected, CCCP treatment depolarized the MMP because of its ability to facilitate proton reflux across the inner mitochondrial membrane, as reported by the literature (Miyazono et al., 2018). Only 1 µM and 0.025 µM concentrations showed significant differences from the control.

In accordance with this study, Shen et al. (2003) showed that CCCP can accelerate the oxygen consumption. Oxygen consumption was significantly increased when CCCP content was around 1 µM and 5 µM. This led to a decrease in the in-well oxygen concentration below 0. A possible explanation for this could be that the dissolvement of Na_2SO_3 did not lead to a complete oxygen-free solution, even if oversaturated. This could result from the diffusion of oxygen back into the wells before the measurements (the solution was approximately 30 minutes on the plate before the experiments were conducted) or temperature drifts in the plate reader. As shown by the data, higher concentrations stopped the oxygen consumption. Other studies linked this to the stop of the cellular respiration (Shen et al., 2003).

4.1.3 Influence of Oligomycin Inhibition

Unexpectedly, oligomycin did not significantly affect the neuroblastoma cells used. No deviations from control were observed in both, OxoPlate® and JC-1 measurements. No explanation for this data could be found in the literature for the used neuroblastoma cells. Other studies with cancer cells show that oligomycin stops the respiration after an hour in most cancer cell lines and leads to an accelerated glycolysis rate after six hours (Hao et al., 2010). This adaption of cancer cells, to shift from energy production by oxidative phosphorylation to aerobic glycolysis, is called the Warburg effect. Even in the presence of oxygen some cancer cells prefer to derive their energy from converting glucose to lactate and can overcome cellular stressors like hypoxia or evade cell death initiated by mitochondrial dysfunction (Hao et al., 2010). Although the cells used were neuroblastoma cells, it is not likely that we would have observed that shift, given the chosen time spans of the experiments (at most 35 minutes). Zimmermann et al. (2017) showed a strong hyperpolarization of the MMP in N18TG2 cells, but unexpectedly no effects of oligomycin were observed in this study.

4.2 Effects of THC

The red/green ratio of THC-treated cells was significantly decreased after four hours. The institute previously obtained findings through JC-1 measurements. Cells treated with THC over 48 hours showed a mean decrease of 30% in the red/green ratio compared to untreated control cells. THC also depolarized the MMP in other studies and uncoupling abilities have been suggested (Sarafian et al., 2003). The data of this study indicates that the membrane depolarization by THC occurs slowly or is a secondary effect, for instance, due to the formation of superoxide radicals, which are able to damage the mitochondria successively.

4.2.1 Effects of THC on Rotenone-Induced Toxicity

The effects of the rotenone-induced toxicity were likewise observed in the experiments with THC. THC-treated cells showed a small but significant increase in the red/green ratio upon rotenone addition. Upon further inspection of the data, the significant difference in the MMP of THC-treated cells that received the inhibitor rotenone was only observed in one experiment. Therefore, the significance was only a spurious correlation, and no significant differences were observed in OxoPlate® and JC-1 measurements. Data related to the effects of THC on rotenone-induced toxicity is not available. The findings of this study do not support the idea that THC has significant counteractive properties against complex I inhibition by rotenone.

4.2.2 Effects of THC on CCCP-induced Toxicity

THC treatment did not significantly affect the change of the MMP induced by CCCP. Treated and untreated cells reacted very similarly.

CCCP accelerated the oxygen consumption in treated and untreated cells. Other studies showed that oxygen consumption was reduced by THC (Fišar et al., 2014). The faster and more precise response in THC-treated cells could be attributed to changes that THC induces in membrane dynamic properties and fluidity by its integration into lipid bilayers

(Mavromoustakos & Daliani, 1999; Tiburu et al., 2007). The changes in the membrane dynamic could facilitate the diffusion of CCCP and enhance its uncoupling abilities. The author proposes this, and as of today, no explanation for this effect can be found in the literature.

Variability of data obtained from mammalian cell cultures is expected. It can be attributed to various reasons, including differences in cell media ingredients (e.g., FBS) or the physiology of the cells on the experiment day (Stein, 2007; Wright Muelas et al., 2018). Although there is not one single explanation for the variance, FBS or bovine serum albumin (BSA) content can also interfere with CCCP treatment, as suggested by recent findings (Soutar et al., 2019). In OxoPlate® experiments, complete removal of the cell medium could only be ensured by washing and subsequent re-centrifugation of cells, significantly affecting cell viability. Therefore FBS/BSA content could have differed between experiments, but only to a minimal extent that would most likely not explain the data variation.

OxoPlate® data variation could have been reduced by measuring and calculating the oxygen consumption rate without O_2-limiting conditions rather than assessing the oxygen content in the well. Problems, such as wells with oxygen contents below 0, could have been avoided. Different oxygen concentrations at the beginning of the experiments are likely attributed to varying temperatures of the PBS at different times, diffusion of oxygen out of the wells before the addition of the cells, or longer initializing times of the plate reader before the first measurement (in which the cells consumed oxygen). This could also have been avoided by calculating the oxygen consumption rate, but since this study aimed to show if there are meaningful differences between treatment groups, assessing the oxygen content was sufficient.

In the JC-1 data, high variation was observed for the determination of effective concentrations of modulators of the ETC. Unfortunately, an incorrect excitation wavelength (280 nm instead of the recommended 488 nm) was used. Studies found low responses of JC-1 dye for excitation wavelengths under 400 nm (Perelman et al., 2012). Additionally, 280 nm is in the region of maximal absorption of proteins (Schmid, 2001). High levels of bleaching would have been expected, but surprisingly the bleaching factor remained close to 1 for the majority of measurements, possibly attributed to the protein absorbance. Notably, the bleaching factor did not fulfill its purpose as a normalization method. Since it accounts for the decay of the green JC-1 monomer, it should always be < 1 (as it is multiplied by the red/green ratio), which was not always in agreement with the data of this study. Bleaching factors in this study usually

remained around 0.97 and 1.02, but sometimes bleaching factors over 1.57 and under 0.95 were observed. Exceptionally high bleaching factors were observed right after the inhibitor addition, possibly due to bleaching of the JC-1 dye during the treatment caused by UV radiation. The addition of the JC-1 dye and the washing steps of the plate were performed in the dark. This was not possible for the inhibitor treatment because the addition occurred directly at the reader, which was positioned in a lab frequently used by other researchers. In subsequent experiments, complete darkening of the room will be necessary to obtain reliable data. Additionally, it might be better to obtain mean bleaching factors from multiple measurements of untreated cells rather than calculate it for every row of every measurement. It cannot be excluded that the JC-1 data variation is caused by the excitation with the wrong wavelength; nevertheless, there were effects observed that must be validated in experiments using correct parameters.

The methods used in this study seem to be suitable since the determination of effective concentrations of modulators of the ETC led to results that were in accordance with the literature, except for oligomycin, which did not influence the cells used. This study found no significant effect of THC on the reaction of mitochondria to the modulators used. Previous studies, e.g. by the institute (Pöhn et al., 2012), demonstrated neuroprotective properties of THC against rotenone-induced toxicity. These effects could be attributed to influences of THC that are independent from the mitochondria, or undetectable by the methods due to the chosen time spans and comparison of oxygen concentrations at certain time points instead of oxygen consumption rates.

5 Conclusion

THC treatment had only minimal effects on the sensitivity of neuroblastoma cells to certain ETC modulators. As reported by other studies, the depolarization of the MMP upon THC addition was observed. This effect was relatively small, with a decrease of the MMP of about 6 % compared to the control. This might be due to a slow depolarization of the MMP after THC treatment. Another explanation that cannot be ruled out is that THC could act on other parts of the cell and leads to a time-delayed alteration of the MMP.

Notably, this study did not observe major mitochondrial impairment following THC treatment. This suggests that THC does not damage mitochondria to a great extent.

Although differences in the reaction of THC-treated and -untreated cells were minor, THC might influence CCCP-induced toxicity and help CCCP pass through the inner mitochondrial membrane. This effect cannot be explained with the literature or the data of this study, and further investigation is required to explain those results.

No changes in the MMP could be observed in THC and control cells upon inhibition of the complex I by rotenone. Its inhibition of the ETC was instant, as supported by the OxoPlate® data. The lack of alteration of the MMP could be attributed to a slow depolarization of the membrane. Another explanation could be that JC-1, when excited with 280 nm, might not be reliable enough to observe small changes in the MMP, given the high variance of the data. Nevertheless, the establishment of the methods was accomplished through the determination of inhibitory concentrations of certain modulators of functions of the ETC.

Consequently, JC-1 data should be validated by repeating the experiments with the correct wavelength or using other MMP markers, such as rhodamine-123 or tetramethyl rhodamine methyl and ethyl esters. To establish if and where THC has protective properties on the ETC in neurons, other complex inhibitors must be tested to determine if THC treatment significantly affects their toxicity. In any case, the data of this study regarding the CCCP treatment suggests that THC has a direct impact on mitochondria.

6 References

Alberts, B., Johnson, A., Lewis, J., Morgan, D., Raff, M., Roberts, K., & Walter, P. (2015). *Molecular Biology of the Cell* (J. Wilson & T. Hunt (eds.); Sixth Edit). W.W. Norton & Company. https://doi.org/10.1201/9781315735368

Andre, C. M., Hausman, J.-F., & Guerriero, G. (2016). Cannabis sativa: The Plant of the Thousand and One Molecules. *Frontiers in Plant Science*, *7*(FEB), 19. https://doi.org/10.3389/fpls.2016.00019

Antoniel, M., Giorgio, V., Fogolari, F., Glick, G. D., Bernardi, P., & Lippe, G. (2014). The Oligomycin-Sensitivity Conferring Protein of Mitochondrial ATP Synthase: Emerging New Roles in Mitochondrial Pathophysiology. *International Journal of Molecular Sciences*, *15*(5), 7513. https://doi.org/10.3390/IJMS15057513

Artika, I. M. (2019). Current understanding of structure, function and biogenesis of yeast mitochondrial ATP synthase. *Journal of Bioenergetics and Biomembranes*, *51*(5), 315–328. https://doi.org/10.1007/s10863-019-09809-4

Bender, T., & Martinou, J. C. (2016). The mitochondrial pyruvate carrier in health and disease: To carry or not to carry? *Biochimica et Biophysica Acta - Molecular Cell Research*, *1863*(10), 2436–2442. https://doi.org/10.1016/j.bbamcr.2016.01.017

Chandel, N. S. (2010). Mitochondrial complex III: An essential component of universal oxygen sensing machinery? *Respiratory Physiology and Neurobiology*, *174*(3), 175–181. https://doi.org/10.1016/j.resp.2010.08.004

Cooray, R., Gupta, V., & Suphioglu, C. (2020). Current Aspects of the Endocannabinoid System and Targeted THC and CBD Phytocannabinoids as Potential Therapeutics for Parkinson's and Alzheimer's Diseases: a Review. *Molecular Neurobiology*, *57*(11), 4878–4890. https://doi.org/10.1007/s12035-020-02054-6

Cristino, L., Bisogno, T., & Di Marzo, V. (2020). Cannabinoids and the expanded endocannabinoid system in neurological disorders. *Nature Reviews Neurology*, *16*(1), 9–29. https://doi.org/10.1038/s41582-019-0284-z

Cui, Q., Wen, S., & Huang, P. (2017). Targeting cancer cell mitochondria as a therapeutic approach: recent updates. *Future Medicinal Chemistry*, *9*(9), 929–949. https://doi.org/10.4155/fmc-2017-0011

De Petrocellis, L., & Di Marzo, V. (2009). An introduction to the endocannabinoid system: from the early to the latest concepts. *Best Practice and Research: Clinical Endocrinology and Metabolism*, *23*(1), 1–15. https://doi.org/10.1016/J.BEEM.2008.10.013

Di Marzo, V., & Piscitelli, F. (2015). The Endocannabinoid System and its Modulation by Phytocannabinoids. *Neurotherapeutics*, *12*(4), 692–698. https://doi.org/10.1007/s13311-015-0374-6

Fišar, Z., Singh, N., & Hroudová, J. (2014). Cannabinoid-induced changes in respiration of brain mitochondria. *Toxicology Letters*, *231*(1), 62–71. https://doi.org/10.1016/j.toxlet.2014.09.002

Guo, H., & Rubinstein, J. L. (2022). Structure of ATP synthase under strain during catalysis. *BioRxiv*, *2022*, 1–22. https://doi.org/10.1038/s41467-022-29893-2

Hao, W., Chang, C.-P. B., Tsao, C.-C., & Xu, J. (2010). Oligomycin-induced Bioenergetic Adaptation in Cancer Cells with Heterogeneous Bioenergetic Organization. *Journal of Biological Chemistry*, *285*(17), 12647–12654. https://doi.org/10.1074/jbc.M109.084194

Hearne, A., Chen, H., Monarchino, A., & Wiseman, J. S. (2020). Oligomycin-induced proton uncoupling. *Toxicology in Vitro*, *67*(June), 104907. https://doi.org/10.1016/j.tiv.2020.104907

Heinz, S., Freyberger, A., Lawrenz, B., Schladt, L., Schmuck, G., & Ellinger-Ziegelbauer, H. (2017). Mechanistic Investigations of the Mitochondrial Complex I Inhibitor Rotenone in the Context of Pharmacological and Safety Evaluation. *Scientific Reports 2017 7:1*, *7*(1), 1–13. https://doi.org/10.1038/srep45465

Herbert-Chatelain, E., Marsicano, G., & Desprez, T. (2017). Endocannabinoids and Lipid Mediators in Brain Functions. In M. Melis (Ed.), *Endocannabinoids and Lipid Mediators in Brain Functions*. Springer International Publishing. https://doi.org/10.1007/978-3-319-

57371-7

Joshi, N., & Onaivi, E. S. (2019). Endocannabinoid System Components: Overview and Tissue Distribution. *Advances in Experimental Medicine and Biology*, *1162*, 1–12. https://doi.org/10.1007/978-3-030-21737-2_1

Kampjut, D., & Sazanov, L. A. (2020). The coupling mechanism of mammalian respiratory complex I. *Science*, *370*(6516), 1–18. https://doi.org/10.1126/SCIENCE.ABC4209

Kane, M. S., Paris, A., Codron, P., Cassereau, J., Procaccio, V., Lenaers, G., Reynier, P., & Chevrollier, A. (2018). Current mechanistic insights into the CCCP-induced cell survival response. *Biochemical Pharmacology*, *148*, 100–110. https://doi.org/10.1016/j.bcp.2017.12.018

Keuper, M., Jastroch, M., Yi, C. X., Fischer-Posovszky, P., Wabitsch, M., Tschöp, M. H., & Hofmann, S. M. (2014). Spare mitochondrial respiratory capacity permits human adipocytes to maintain ATP homeostasis under hypoglycemic conditions. *FASEB Journal*, *28*(2), 761–770. https://doi.org/10.1096/fj.13-238725

Kirtonia, A., Sethi, G., & Garg, M. (2020). The multifaceted role of reactive oxygen species in tumorigenesis. *Cellular and Molecular Life Sciences*, *77*(22), 4459–4483. https://doi.org/10.1007/s00018-020-03536-5

Koncha, R. R., Ramachandran, G., Sepuri, N. B. V., & Ramaiah, K. V. A. (2021). CCCP-induced mitochondrial dysfunction – characterization and analysis of integrated stress response to cellular signaling and homeostasis. *FEBS Journal*, *288*(19), 5737–5754. https://doi.org/10.1111/febs.15868

Kwon, K. Y., Viollet, B., & Yoo, O. J. (2011). CCCP induces autophagy in an AMPK-independent manner. *Biochemical and Biophysical Research Communications*, *416*(3–4), 343–348. https://doi.org/10.1016/j.bbrc.2011.11.038

Li, N., Ragheb, K., Lawler, G., Sturgis, J., Rajwa, B., Melendez, J. A., & Robinson, J. P. (2003). Mitochondrial complex I inhibitor rotenone induces apoptosis through enhancing mitochondrial reactive oxygen species production. *Journal of Biological Chemistry*, *278*(10), 8516–8525. https://doi.org/10.1074/jbc.M210432200

Lipina, C., Irving, A. J., & Hundal, H. S. (2014). Mitochondria: a possible nexus for the regulation of energy homeostasis by the endocannabinoid system? *American Journal of Physiology-Endocrinology and Metabolism*, *307*(1), E1–E13. https://doi.org/10.1152/ajpendo.00100.2014

Lowe, H., Toyang, N., Steele, B., Bryant, J., & Ngwa, W. (2021). The Endocannabinoid System: A Potential Target for the Treatment of Various Diseases. *International Journal of Molecular Sciences*, *22*(17), 9472. https://doi.org/10.3390/ijms22179472

Lucas, C. J., Galettis, P., & Schneider, J. (2018). The pharmacokinetics and the pharmacodynamics of cannabinoids. *British Journal of Clinical Pharmacology*, *84*(11), 2477–2482. https://doi.org/10.1111/bcp.13710

Lutz, B. (2020). Neurobiology of cannabinoid receptor signaling. *Dialogues in Clinical Neuroscience*, *22*(3), 207–222. https://doi.org/10.31887/DCNS.2020.22.3/blutz

Maroon, J., & Bost, J. (2018). Review of the neurological benefits of phytocannabinoids. *Surgical Neurology International*, *9*(1), 91. https://doi.org/10.4103/sni.sni_45_18

Mavromoustakos, T., & Daliani, I. (1999). Effects of cannabinoids in membrane bilayers containing cholesterol. *Biochimica et Biophysica Acta - Biomembranes*, *1420*(1–2), 252–265. https://doi.org/10.1016/S0005-2736(99)00106-6

Mills, E. L., Kelly, B., Logan, A., Costa, A. S. H., Varma, M., Bryant, C. E., Tourlomousis, P., Däbritz, J. H. M., Gottlieb, E., Latorre, I., Corr, S. C., McManus, G., Ryan, D., Jacobs, H. T., Szibor, M., Xavier, R. J., Braun, T., Frezza, C., Murphy, M. P., & O'Neill, L. A. (2016). Succinate Dehydrogenase Supports Metabolic Repurposing of Mitochondria to Drive Inflammatory Macrophages. *Cell*, *167*(2), 457-470.e13. https://doi.org/10.1016/j.cell.2016.08.064

Miyazono, Y., Hirashima, S., Ishihara, N., Kusukawa, J., Nakamura, K. I., & Ohta, K. (2018). Uncoupled mitochondria quickly shorten along their long axis to form indented spheroids, instead of rings, in a fission-independent manner. *Scientific Reports*, *8*(1), 1–14. https://doi.org/10.1038/s41598-017-18582-6

Moon, Y., Lee, K. H., Park, J.-H., Geum, D., & Kim, K. (2005). Mitochondrial membrane

depolarization and the selective death of dopaminergic neurons by rotenone: protective effect of coenzyme Q 10. *J. Neurochem*, *93*, 1199–1208. https://doi.org/10.1111/j.1471-4159.2005.03112.x

Mpumi, N., Mtei, K., Machunda, R., & Ndakidemi, P. A. (2016). The Toxicity, Persistence and Mode of Actions of Selected Botanical Pesticides in Africa against Insect Pests in Common Beans, <i>P. vulgaris</i>: A Review. *American Journal of Plant Sciences*, *07*(01), 138–151. https://doi.org/10.4236/AJPS.2016.71015

Nadal, X., del Río, C., Casano, S., Palomares, B., Ferreiro-Vera, C., Navarrete, C., Sánchez-Carnerero, C., Cantarero, I., Bellido, M. L., Meyer, S., Morello, G., Appendino, G., & Muñoz, E. (2017). Tetrahydrocannabinolic acid is a potent PPARγ agonist with neuroprotective activity. *British Journal of Pharmacology*, *174*(23), 4263–4276. https://doi.org/10.1111/bph.14019

Nolfi-Donegan, D., Braganza, A., & Shiva, S. (2020). Mitochondrial electron transport chain: Oxidative phosphorylation, oxidant production, and methods of measurement. *Redox Biology*, *37*, 101674. https://doi.org/10.1016/j.redox.2020.101674

Nunn, A., Guy, G., & Bell, J. D. (2012). Endocannabinoids in neuroendopsychology: Multiphasic control of mitochondrial function. *Philosophical Transactions of the Royal Society B: Biological Sciences*, *367*(1607), 3342–3352. https://doi.org/10.1098/rstb.2011.0393

Nunnari, J., & Suomalainen, A. (2012). Mitochondria: in sickness and in health. *Cell*, *148*(6), 1145–1159. https://doi.org/10.1016/j.cell.2012.02.035

Perelman, A., Wachtel, C., Cohen, M., Haupt, S., Shapiro, H., & Tzur, A. (2012). JC-1: alternative excitation wavelengths facilitate mitochondrial membrane potential cytometry. *Cell Death & Disease*, *3*(11), e430. https://doi.org/10.1038/cddis.2012.171

Plášek, J., Babuka, D., & Hoefer, M. (2017). H+ translocation by weak acid uncouplers is independent of H+ electrochemical gradient. *Journal of Bioenergetics and Biomembranes*, *49*(5), 391–397. https://doi.org/10.1007/s10863-017-9724-x

Pöhn, B., Krewenka, C., Kranner, B., Duvigneau, J., Rausch, W., & Moldzio, R. (2012).

Phytocannabinoids tetrahydrocannabinol and cannabidiol act against rotenone induced damages in murine cell cultures. *Planta Medica*, *78*(11), PD171. https://doi.org/10.1055/s-0032-1320529

Radad, K., Al-Shraim, M., Al-Emam, A., Wang, F., Kranner, B., Rausch, W. D., & Moldzio, R. (2019). Rotenone: from modelling to implication in Parkinson's disease. *Folia Neuropathologica*, *57*(4), 317–326. https://doi.org/10.5114/FN.2019.89857

Radad, K., Rausch, W.-D., & Gille, G. (2006). Rotenone induces cell death in primary dopaminergic culture by increasing ROS production and inhibiting mitochondrial respiration. *Neurochemistry International*, *49*(4), 379–386. https://doi.org/10.1016/j.neuint.2006.02.003

Rimmerman, N., Ben-Hail, D., Porat, Z., Juknat, A., Kozela, E., Daniels, M. P., Connelly, P. S., Leishman, E., Bradshaw, H. B., Shoshan-Barmatz, V., & Vogel, Z. (2013). Direct modulation of the outer mitochondrial membrane channel, voltage-dependent anion channel 1 (VDAC1) by cannabidiol: a novel mechanism for cannabinoid-induced cell death. *Cell Death & Disease*, *4*(12), e949. https://doi.org/10.1038/cddis.2013.471

Ruas, J. S., Siqueira-Santos, E. S., Amigo, I., Rodrigues-Silva, E., Kowaltowski, A. J., & Castilho, R. F. (2016). Underestimation of the Maximal Capacity of the Mitochondrial Electron Transport System in Oligomycin-Treated Cells. *PLOS ONE*, *11*(3), e0150967. https://doi.org/10.1371/journal.pone.0150967

Sarafian, T. A., Kouyoumjian, S., Khoshaghideh, F., Tashkin, D. P., & Roth, M. D. (2003). Δ 9 -Tetrahydrocannabinol disrupts mitochondrial function and cell energetics. *American Journal of Physiology-Lung Cellular and Molecular Physiology*, *284*(2), L298–L306. https://doi.org/10.1152/ajplung.00157.2002

Schlag, A. K., O'Sullivan, S. E., Zafar, R. R., & Nutt, D. J. (2021). Current controversies in medical cannabis: Recent developments in human clinical applications and potential therapeutics. *Neuropharmacology*, *191*(May), 108586. https://doi.org/10.1016/j.neuropharm.2021.108586

Schmid, F. (2001). Biological Macromolecules: UV-visible Spectrophotometry. In *eLS* (pp. 1–4). Wiley. https://doi.org/10.1038/npg.els.0003142

Shen, J., Khan, N., Lewis, L. D., Armand, R., Grinberg, O., Demidenko, E., & Swartz, H. (2003). Oxygen consumption rates and oxygen concentration in Molt-4 cells and their mtDNA depleted (ρ0) mutants. *Biophysical Journal*, *84*(2 I), 1291–1298. https://doi.org/10.1016/S0006-3495(03)74944-3

Sies, H., & Jones, D. P. (2020). Reactive oxygen species (ROS) as pleiotropic physiological signalling agents. *Nature Reviews Molecular Cell Biology*, *21*(7), 363–383. https://doi.org/10.1038/s41580-020-0230-3

Sousa, J. S., D'Imprima, E., & Vonck, J. (2018). Mitochondrial Respiratory Chain Complexes. In *Subcellular Biochemistry* (Vol. 87, pp. 167–227). https://doi.org/10.1007/978-981-10-7757-9_7

Soutar, M. P. M., Kempthorne, L., Annuario, E., Luft, C., Wray, S., Ketteler, R., Ludtmann, M. H. R., & Plun-Favreau, H. (2019). FBS/BSA media concentration determines CCCP's ability to depolarize mitochondria and activate PINK1-PRKN mitophagy. *Autophagy*, *15*(11), 2002–2011. https://doi.org/10.1080/15548627.2019.1603549

Stein, A. (2007). Decreasing variability in your cell culture. *BioTechniques*, *43*(2), 228–229. https://doi.org/10.2144/000112561

Tada-Oikawa, S., Hiraku, Y., Kawanishi, M., & Kawanishi, S. (2003). Mechanism for generation of hydrogen peroxide and change of mitochondrial membrane potential during rotenone-induced apoptosis. *Life Sciences*, *73*(25), 3277–3288. https://doi.org/10.1016/j.lfs.2003.06.013

Telford, J. E., Kilbride, S. M., & Davey, G. P. (2009). Complex I Is Rate-limiting for Oxygen Consumption in the Nerve Terminal. *Journal of Biological Chemistry*, *284*(14), 9109–9114. https://doi.org/10.1074/jbc.M809101200

Tiburu, E. K., Bass, C. E., Struppe, J. O., Lorigan, G. A., Avraham, S., & Avraham, H. K. (2007). Structural divergence among cannabinoids influences membrane dynamics: A 2H Solid-State NMR analysis. *Biochimica et Biophysica Acta - Biomembranes*, *1768*(9), 2049–2059. https://doi.org/10.1016/j.bbamem.2007.04.023

Wallace, D. C. (2012). Mitochondria and cancer. *Nature Reviews Cancer*, *12*(10), 685–698.

https://doi.org/10.1038/nrc3365

Wisden, W., Yu, X., & Franks, N. P. (2019). GABA Receptors and the Pharmacology of Sleep. *Handbook of Experimental Pharmacology*, *253*, 279–304. https://doi.org/10.1007/164_2017_56

Won, J. H., Park, S., Hong, S., Son, S., & Yu, J. W. (2015). Rotenone-induced Impairment of Mitochondrial Electron Transport Chain Confers a Selective Priming Signal for NLRP3 Inflammasome Activation. *Journal of Biological Chemistry*, *290*(45), 27425–27437. https://doi.org/10.1074/jbc.M115.667063

Wright Muelas, M., Ortega, F., Breitling, R., Bendtsen, C., & Westerhoff, H. V. (2018). Rational cell culture optimization enhances experimental reproducibility in cancer cells. *Scientific Reports*, *8*(1), 1–16. https://doi.org/10.1038/s41598-018-21050-4

Zhao, R. Z., Jiang, S., Zhang, L., & Yu, Z. Bin. (2019). Mitochondrial electron transport chain, ROS generation and uncoupling (Review). *International Journal of Molecular Medicine*, *44*(1), 3–15. https://doi.org/10.3892/ijmm.2019.4188

Zimmermann, L., Moldzio, R., Vazdar, K., Krewenka, C., & Pohl, E. E. (2017). Nutrient deprivation in neuroblastoma cells alters 4-hydroxynonenal-induced stress response. *Oncotarget*, *8*(5), 8173. https://doi.org/10.18632/ONCOTARGET.14132

Zou, S., & Kumar, U. (2018). Cannabinoid Receptors and the Endocannabinoid System: Signaling and Function in the Central Nervous System. *International Journal of Molecular Sciences*, *19*(3), 833. https://doi.org/10.3390/ijms19030833

7 Figures